

## Wintertime aerosol chemical composition and source apportionment of the organic fraction in the metropolitan area of Paris

M. Crippa<sup>1</sup>, P. F. DeCarlo<sup>1\*</sup>, J. G. Slowik<sup>1</sup>, C. Mohr<sup>1\*\*</sup>, M. F. Heringa<sup>1\*\*\*</sup>, R. Chirico<sup>1\*\*\*\*</sup>, L. Poulain<sup>2</sup>, F. Freutel<sup>3</sup>, J. Sciare<sup>4</sup>, J. Cozic<sup>5</sup>, C. F. Di Marco<sup>6</sup>, M. Elsasser<sup>7,8</sup>, J. B. Nicolas<sup>4</sup>, N. Marchand<sup>9</sup>, E. Abidi<sup>9</sup>, A. Wiedensohler<sup>2</sup>, F. Drewnick<sup>3</sup>, J. Schneider<sup>3</sup>, S. Borrmann<sup>3,10</sup>, E. Nemitz<sup>6</sup>, R. Zimmermann<sup>7,8</sup>, J.-L. Jaffrezo<sup>5</sup>, A. S. H. Prévôt<sup>1</sup>, and U. Baltensperger<sup>1</sup>

[1]{Laboratory of Atmospheric Chemistry, Paul Scherrer Institute, PSI Villigen, 5232, Switzerland}

[2]{Leibniz Institut for Tropospheric Research, Permoserstr 15, 04318, Leipzig, Germany}

[3]{Particle Chemistry Department, Max-Planck-Institute for Chemistry, D-55128 Mainz, Germany}

[4]{Laboratoire des Sciences du Climat et de l'Environnement (LSCE/IPSL), Laboratoire CEA-CNRS-UVSQ, 91191 Gif-sur-Yvette, France}

[5]{UJF – Grenoble 1 / CNRS, Laboratoire de Glaciologie et Géophysique de l'Environnement (LGGE) UMR 5183, Grenoble, F-38041, France}

[6]{Centre for Ecology and Hydrology, Bush Estate, Penicuik, Midlothian, EH26 0QB, United Kingdom}

[7]{Joint Mass Spectrometry Centre, Cooperation Group Comprehensive Molecular Analytics, Helmholtz Zentrum München, Ingolstädter Landstr. 1, 85764 Neuherberg, Germany}

[8]{Joint Mass Spectrometry Centre, Universität Rostock, Institut für Chemie, Lehrstuhl für Analytische Chemie, Dr.-Lorenz-Weg 1, 18059 Rostock}

[9]{Aix-Marseille Université, CNRS, LCE FRE 3416, 13331, Marseille, France}

[10]{Institute for Atmospheric Physics, Johannes Gutenberg University, Mainz, Germany}

[\*]{now at: Department of Civil, Architectural, and Environmental Engineering, Drexel University, Philadelphia, PA, USA, 19104}

[\*\*]{now at: Department of Atmospheric Sciences, University of Washington, Seattle WA 98195, USA}

[\*\*\*]{now at: WIL Research, 5203 DL 's-Hertogenbosch, The Netherlands}

[\*\*\*\*]{now at: Italian National Agency for New Technologies, Energy and Sustainable Economic Development (ENEA), UTAPRAD-DIM, Via E. Fermi 45, 00044 Frascati, Italy}

Correspondence to: A.S.H. Prévôt (andre.prevot@psi.ch)

## SI-1 Measurement sites location

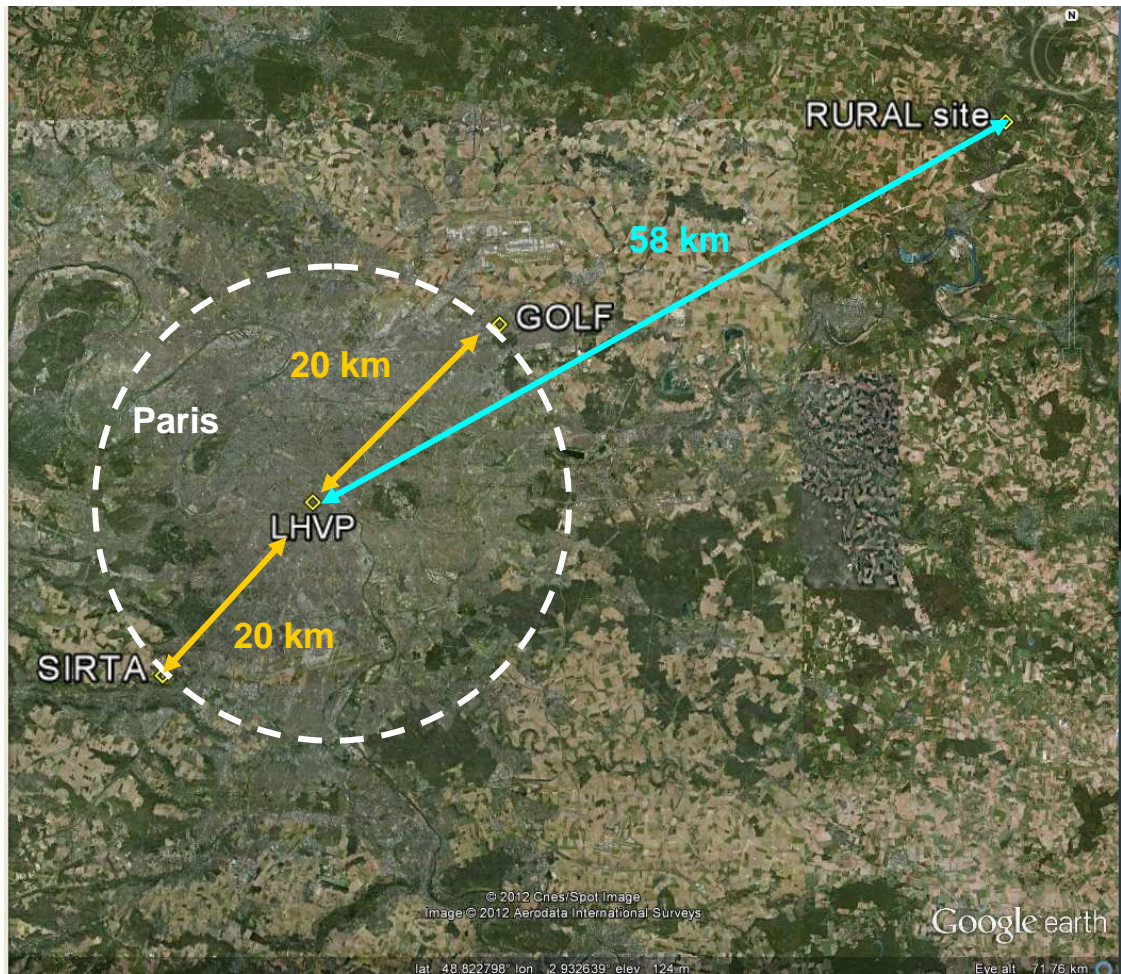


Figure SI-1: Measurement sites location: Google Earth satellite image of the greater Paris region in the Northeastern part of France.

## SI-2 Bounce efficiency estimation

The AMS collection efficiency (CE) has been defined as the product of  $E_b * E_l * E_s$ , where  $E_b$  is the bounce efficiency,  $E_l$  corresponds to the losses in the aerodynamic lenses and  $E_s$  represents the losses due to particles shape (non spherical particles are less efficiently focused compared to spherical ones). Since we assume most of the CE is associated to the bounce efficiency, in the following we will refer to  $E_b$  instead of CE.

The AMS bounce efficiency ( $E_b$ ) depends on particle transmission through the aerodynamic lens, their focusing onto the vaporizer, and the probability of flash vaporization. Therefore  $E_b$  depends on both particle aerodynamic size and composition. For quantitative mass concentrations within the AMS transmission window, the most important consideration is the vaporization probability.  $E_b$  represents the fraction of particles that are vaporized, with other particles bouncing off the heated surface without vaporizing, or vaporizing too slowly for detection (Matthew et al., 2008).

For particles near the mode of the mass distribution,  $E_b$  is primarily affected by the particle composition. Typical values for ambient particles are  $\sim 0.5$ , with higher values observed for acidic particles and particles with high water and/or nitrate content.  $E_b$  has recently been parameterized in terms of these quantities and a parameterization of  $E_b$  as a function of the  $\text{NO}_3$  content has been calculated in this work for comparison purposes (Middlebrook, 2012).

$E_b$  can also be estimated by comparison of AMS data to external measurements. Note that this is not a fully quantitative method of calculating  $E_b$ , as the other instruments may have their own biases or uncertainties. Additionally, such comparisons are complicated by the differences in size-dependent particle transmission between instruments. Because of these complications, we adopt  $E_b=0.5$  unless the comparisons provide evidence to the contrary. Here the AMS inorganic and organic mass concentrations are compared to PILS and off-line filter measurements for the SARTA and LHVP sites with a cutoff of  $\text{PM}_{2.5}$  (Figure SI-2d, Figure SI-2f and Figure SI-4). In addition the AMS estimated volume, calculated assuming a composition-dependent density for the AMS species ( $\text{Org}=1.27 \text{ g/cm}^3$ ;  $\text{SO}_4=1.78 \text{ g/cm}^3$ ;  $\text{NO}_3=1.72 \text{ g/cm}^3$ ;  $\text{NH}_4=1.75 \text{ g/cm}^3$ ;  $\text{Chl}=1.4 \text{ g/cm}^3$ ) (Duplissy et al., 2011), has been related to the measured SMPS (scanning mobility particle sizer) and TDMPS (tandem differential mobility particle sizer) volumes after the subtraction of the estimated BC volume (assuming a density of  $1.77 \text{ g/cm}^3$ ) for the SARTA and LHVP sites (Figure SI-2b and Figure SI-2e). The SMPS large-size cutpoint at SARTA was 453 nm, while the TDMPS cutpoint at LHVP was  $\sim 800$  nm. For the GOLF site the AMS mass is compared to TEOM (tapered-element oscillating microbalance)  $\text{PM}_1$  measurements (Figure SI-2a).

A comparison between total AMS mass and the PM<sub>1</sub> mass concentration measured at the GOLF site by the TEOM-FDMS has been performed. Although the AMS to (TEOM minus MAAP) ratio is slightly lower than 0.5,  $E_b = 0.5$  has been adopted for this dataset due to the higher size cut of the TEOM (PM<sub>1</sub>) and the AMS intercomparison results shown in SI-3. In addition, no NO<sub>3</sub> dependence of  $E_b$  has been identified.

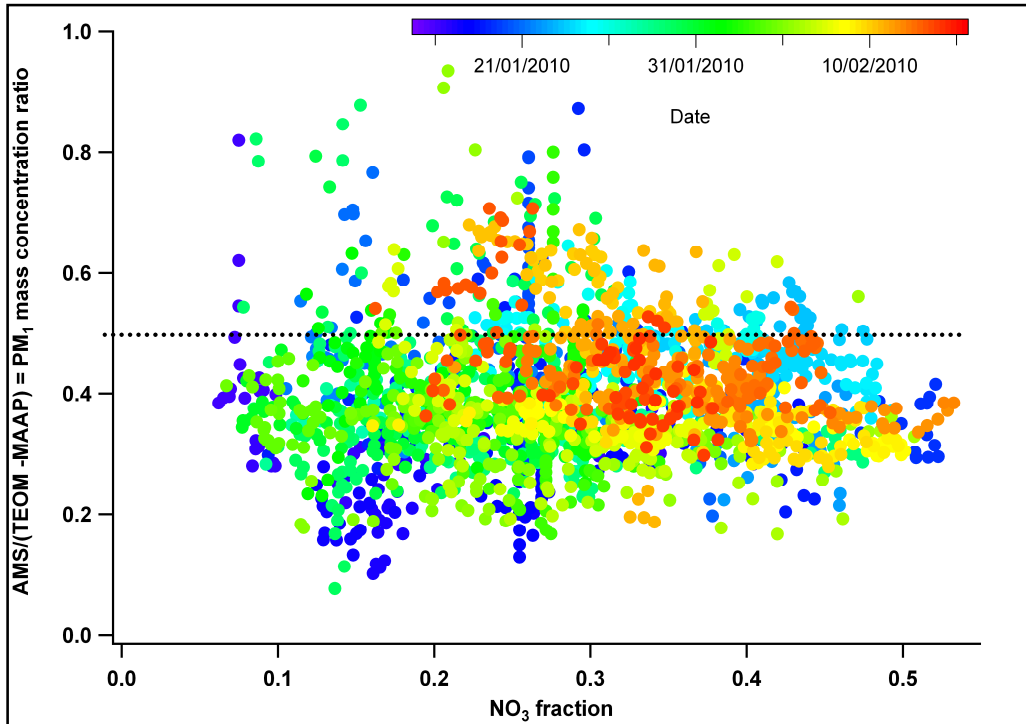


Figure SI-2a:  $E_b$  estimation for the C-ToF at the GOLF site.

From the AMS vs. SMPS subtracted by the BC contribution volume comparison, the  $E_b$  is estimated to be 0.5. Although the two instruments have relatively similar cut points (SMPS cut off=453nm), the apparent presence of two  $E_b$  values (0.5 and 1) during different periods of the campaign are most probably associated to the role of the size distribution and higher mass concentrations which more strongly influence the AMS because of its transmission function for large particles. No  $\text{NO}_3$ -dependent  $E_b$  could be inferred. In addition the comparison with the PILS measurements (PILS cut off equal to  $\text{PM}_{2.5}$ ) shows a good agreement between the two instruments after applying  $E_b=0.5$  (Figure SI-2d). The difference between the AMS and SMPS volumetric ratios is associated to a change in the particles density, as pointed out in Figure SI-2c, affecting the overlapping range of measurements of the two instruments.

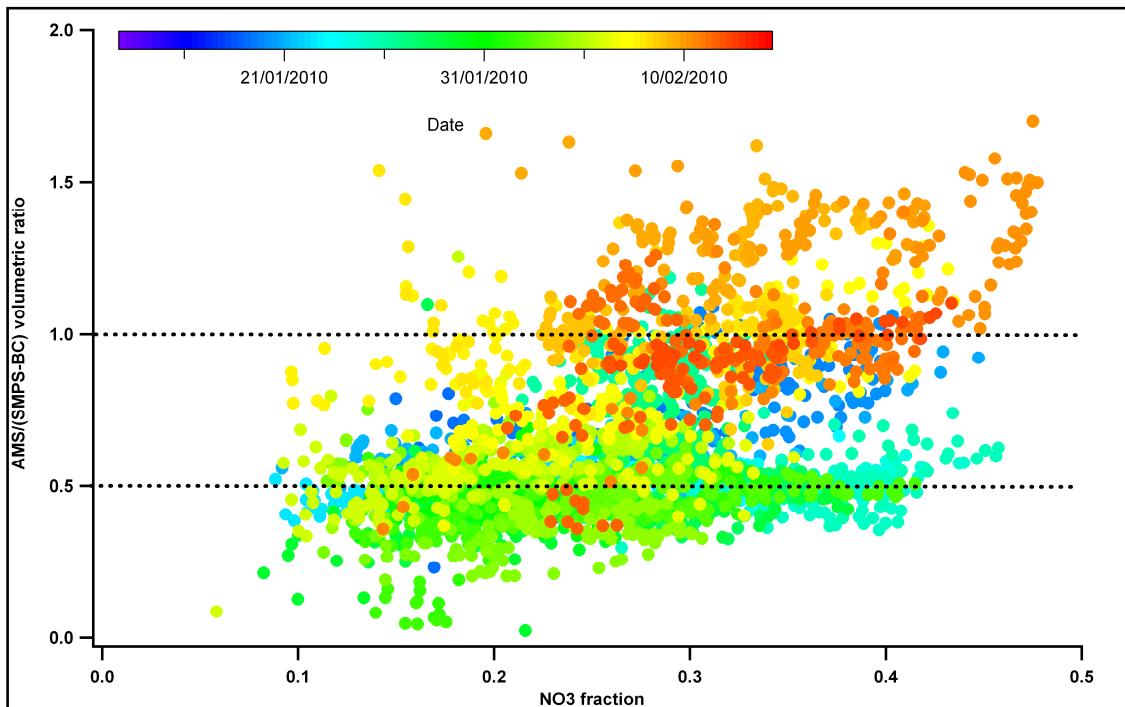


Figure SI-2b:  $E_b$  estimation for the HR-ToF-AMS at the SIRTA site.

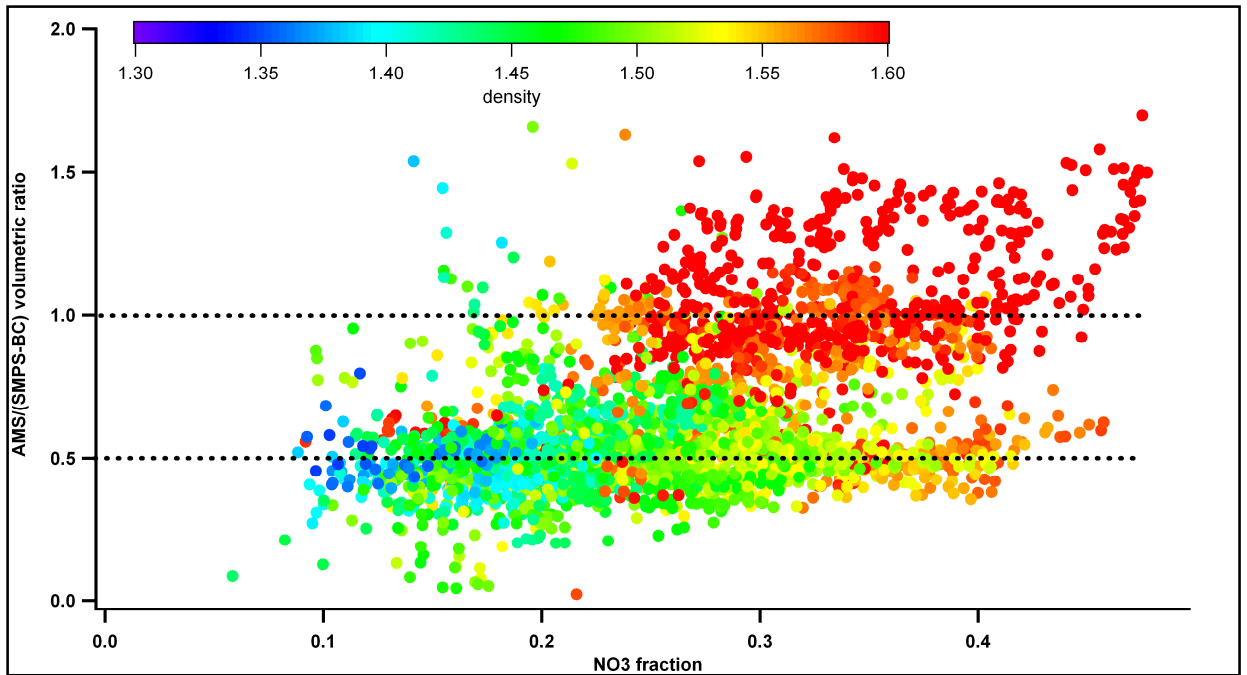


Figure SI-2c:  $E_b$  estimation for the HR-ToF-AMS at the SIRTAsite with the respect of calculated density.

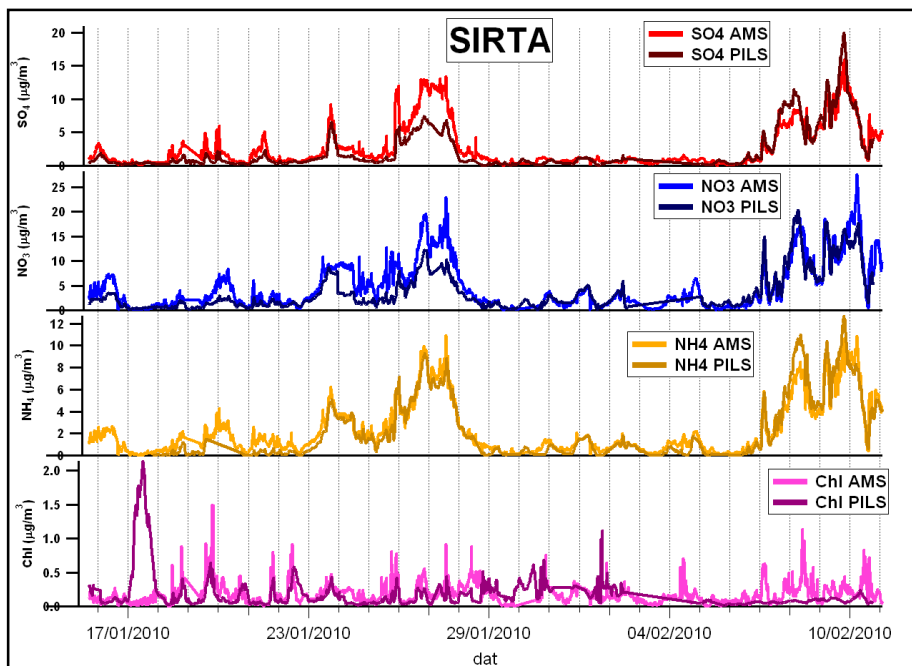


Figure SI-2d: Inorganic species comparison at the SIRTAsite.

A comparison of the AMS-estimated volume (cut off  $PM_{1}$ ) with the TDMPS (cut-off around 800 nm) BC volume subtracted is reported. Additional comparisons of AMS measurements with inorganic species from the PILS (cut off  $PM_{2.5}$ ) have been performed. From the agreements with the volume and inorganic species comparisons, the  $E_b$  has been assumed equal to 0.4.

The application of a  $NO_3$  dependent  $E_b$  which could be inferred from Figure SI-2e (Middlebrook, 2012) causes a significant underestimation of the inorganic AMS species during the high mass concentration events when compared to the PILS measurements (Figure SI-2f).

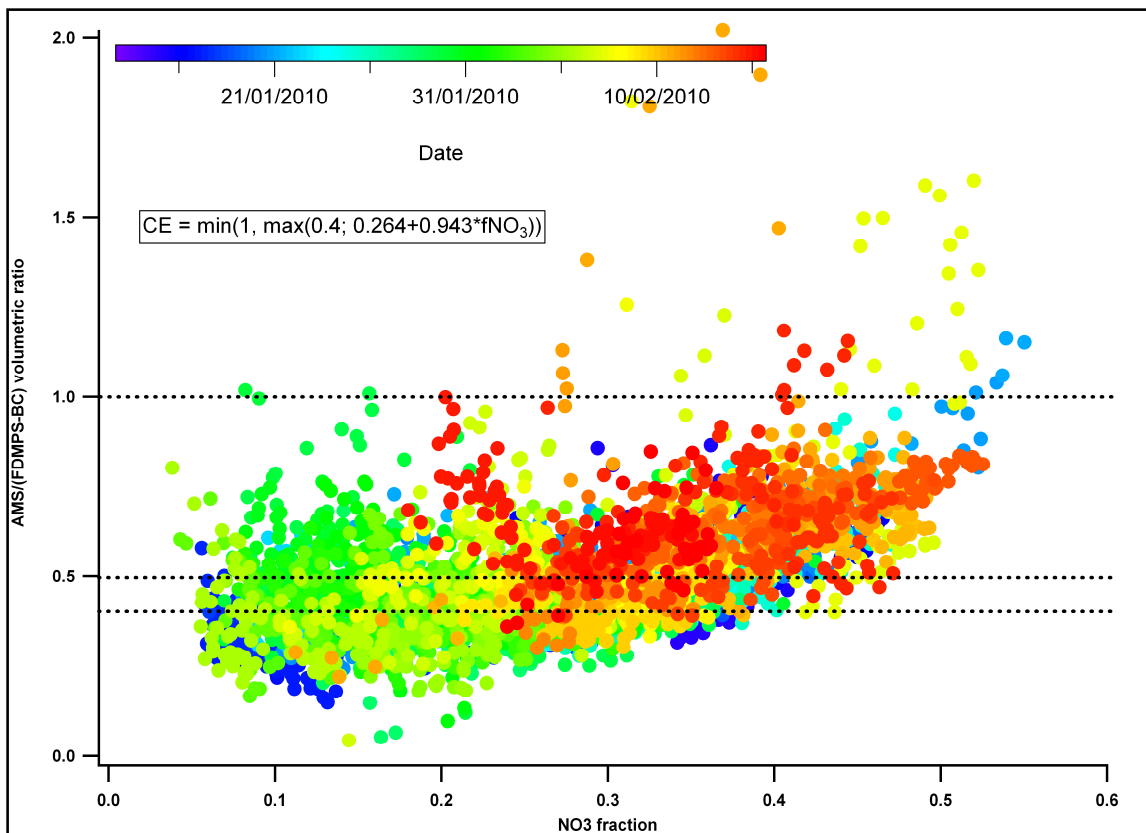


Figure SI-2e:  $E_b$  estimation for the HR-ToF-AMS at the LHVP site.

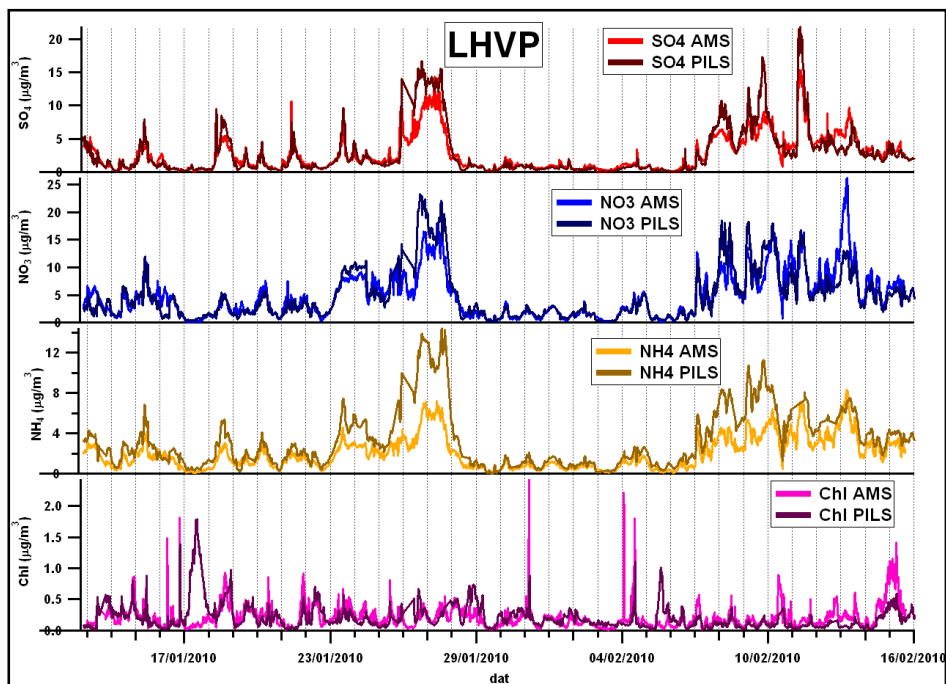


Figure SI-2f: Inorganic species comparison at the LHVP site applying a nitrate dependent  $E_b$  to the AMS data.

### SI-3 AMS intercomparisons

AMS intercomparison exercises were performed during the Paris campaign to determine measurement consistency among the different instruments. The intercomparisons were conducted at the three stationary sites involving also two HR-ToF-AMS deployed in two mobile laboratories. A detailed characterization of these two mobile laboratories can be found in Mohr et al. (2011) and in Drewnick et al. (2012).

In the interpretation of the results, it is necessary to take into account the differences in the inlets and setups (therefore different temperature influence, losses etc.). A similar exercise was performed by Bahreini et al. (2009), and the total AMS variability was estimated at 30% (10% for different inlets, 20% for the ionization efficiency calibrations and 20% for the bounce efficiency).

These comparisons are primarily necessary to identify periods in which significantly different mass concentration levels were measured at the 3 sites during the campaign. Moreover, the comparison of the mass spectra is necessary to evaluate if all the instruments have the same organic fragmentation pattern in order to allow the direct comparison of PMF results. Figures SI-3a, SI-3b, SI-3c, and SI-3d show the AMS species time series and mass spectra for each intercomparison exercise. Although it was not possible to compare directly side by side all the AMS deployed during the campaign, however it is possible to argue that also indirectly all the AMS agree within 30%.

During the whole campaign stationary measurements were performed at the SIRTA site deploying also the PSI mobile laboratory (Mohr et al., 2011), mainly over night or during the not mobile measurements periods. The  $E_b$  of the AMS operating in the PSI mobile laboratory and the one deployed at the SIRTA stationary site were both 0.5. The agreement of the inorganic compounds and the organics fragmentation is very good (maximum 10% of deviation), whereas 30% of difference can be identified in the organics time series.

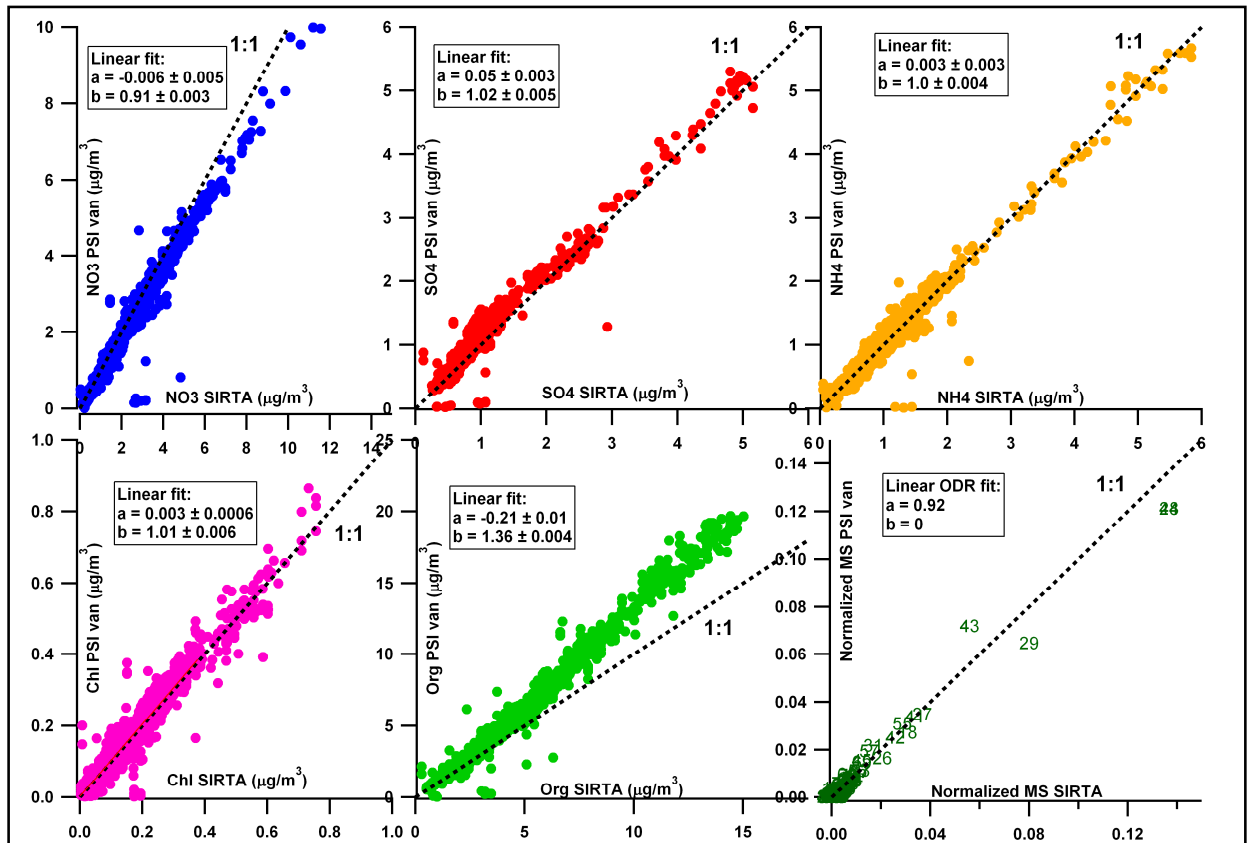


Figure SI-3a: PSI mobile laboratory vs. SIRTA trailer (SIRTA intercomparison during the whole campaign).

During the whole campaign, at the GOLF site several comparisons between the AMS operating at the fixed site and the one deployed in the MPI mobile laboratory (Von der Weiden-Reinmüller, in preparation) were performed.  $E_b$  is for both instruments 0.5. The correlations of the times series and mass spectra are within the uncertainty range (30%). The low ion transmission efficiency of the C-ToF-AMS deployed at the GOLF stationary site has been taken into account with a scaling factor of 1.3 for the organic concentrations after the comparison with contemporary measurements performed with the HR-ToF-AMS deployed at the same location (Freutel et al., 2013).

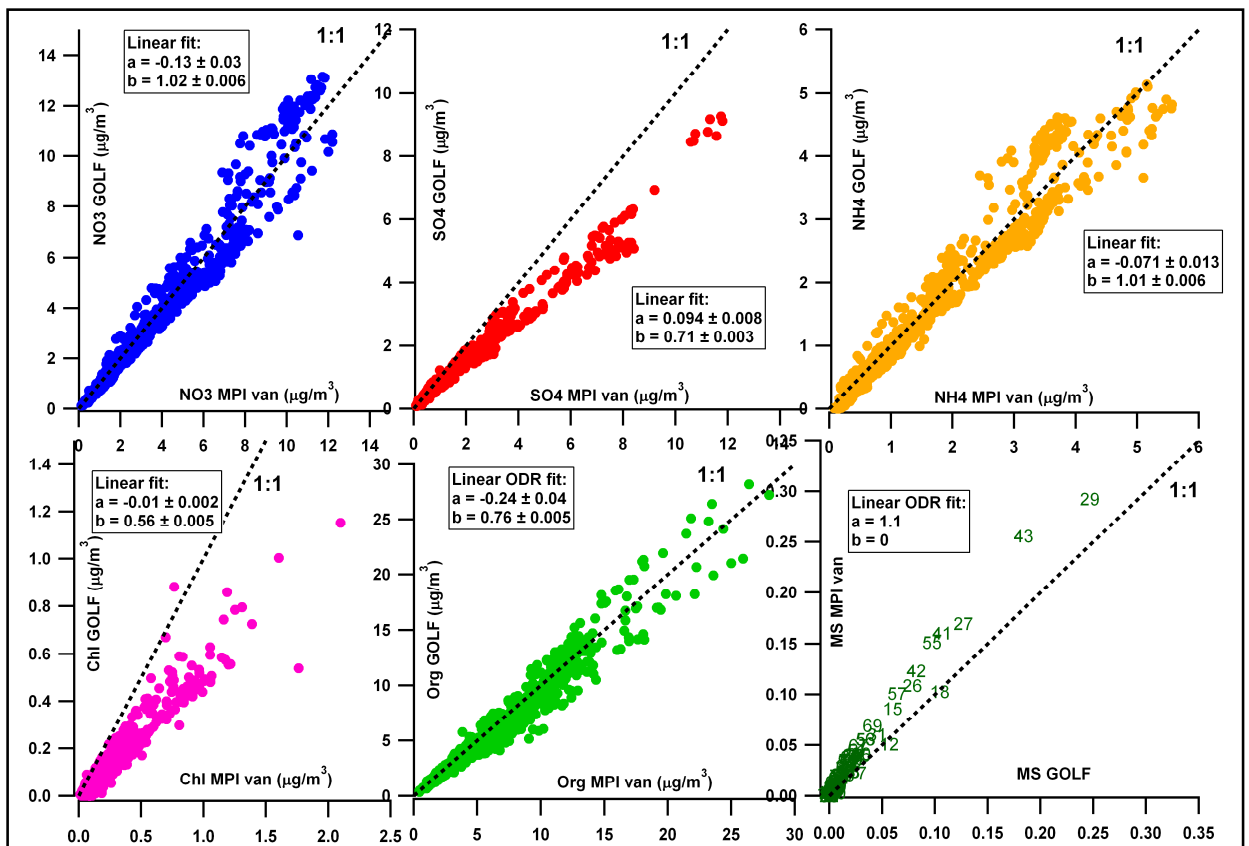


Figure SI-3b: GOLF site comparisons (during the whole campaign).

During this exercise the MPI mobile laboratory and the LHVP stationary AMS were compared.  $E_b$  equal to 0.4 has been assumed for the LHVP AMS and 0.5 for the MPI mobile laboratory instrument. The AMS species time series agree within the uncertainty range (30%) (Bahreini et al., 2009), whereas the organics mass spectra are perfectly coherent.

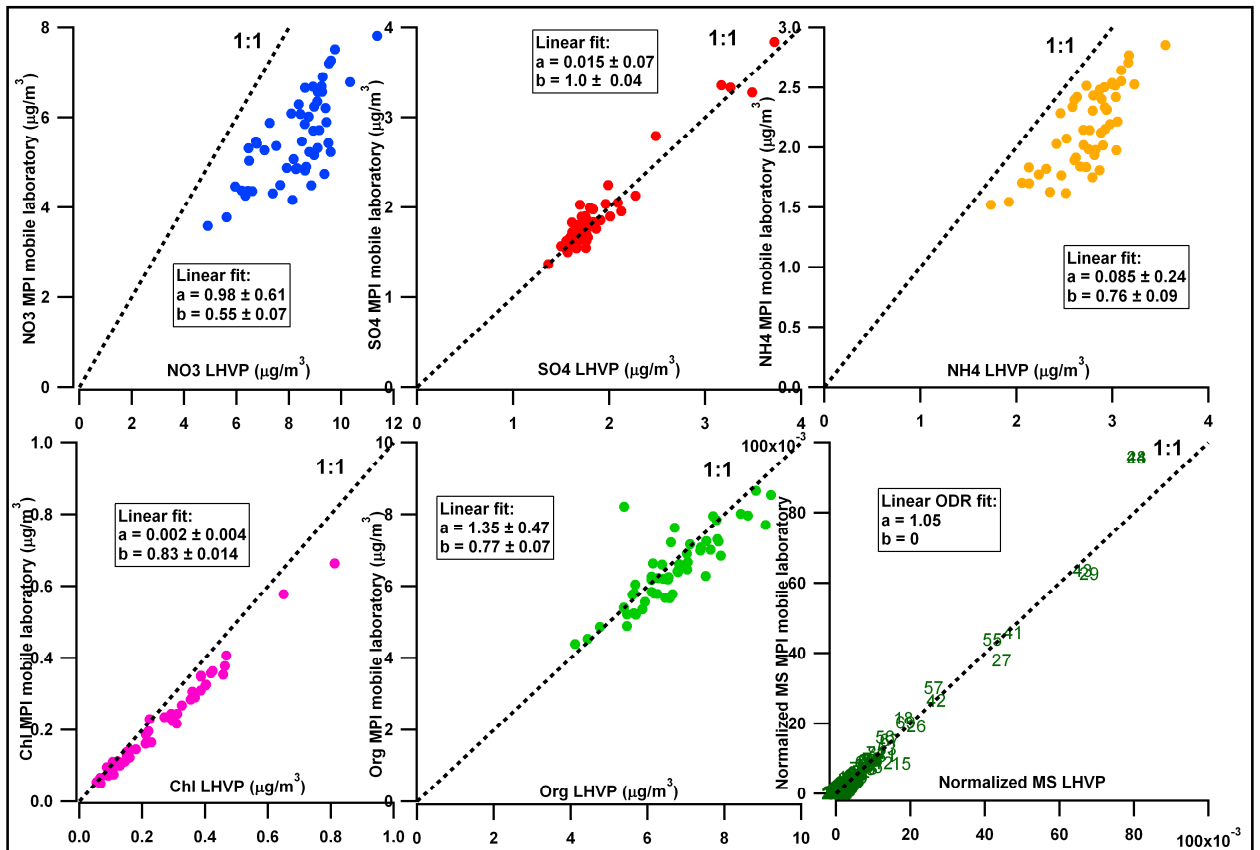


Figure SI-3c: First intercomparison at LHVP site (25 Jan 2010).

A second intercomparison was performed at the LHVP site between the AMS deployed in the PSI mobile laboratory and the LHVP instrument located into the stationary trailer. The applied  $E_b$  for the PSI mobile van AMS is 0.5 and for the LHVP instrument is 0.4. The correlations of the AMS species time series are within 30% of deviation.

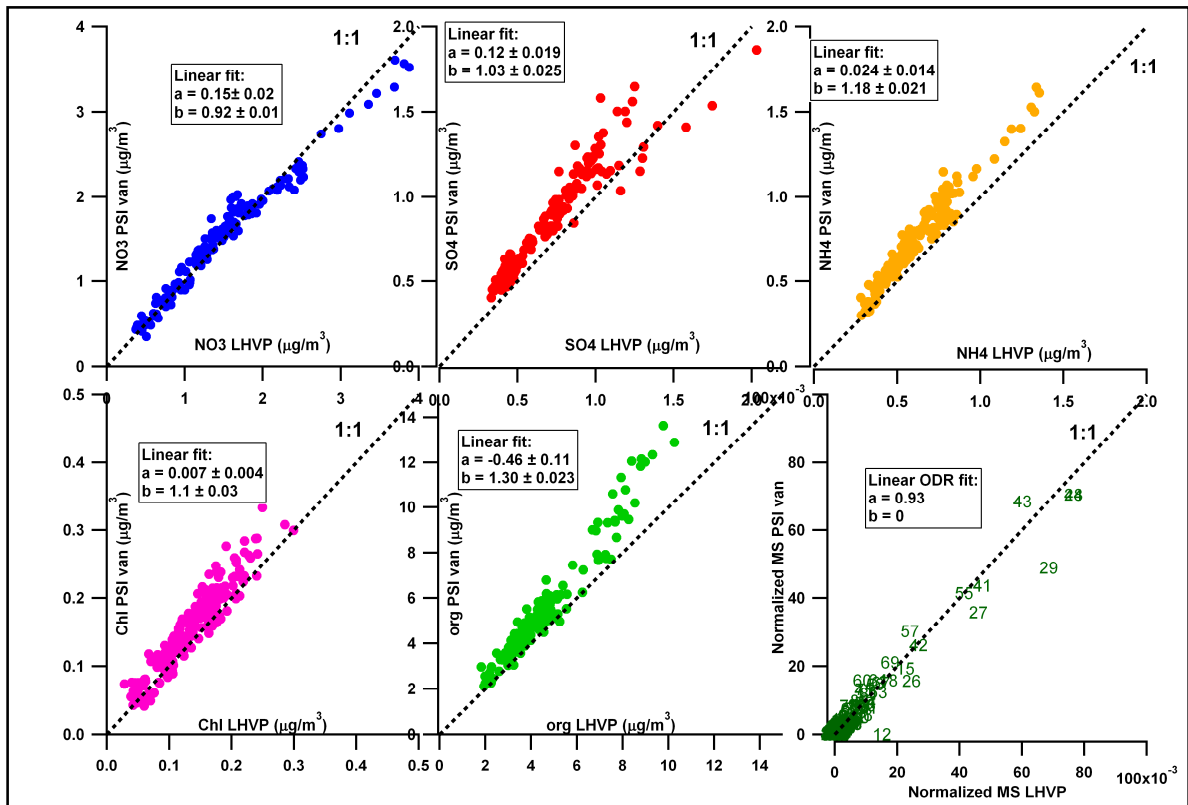


Figure SI-3d: Second intercomparison at LHVP site (1-2 Feb 2010).

## SI-4 Organic carbon (OC) comparison between AMS and filter measurements

In Figure SI-4 comparison between the organic carbon (OC) evaluated using high resolution AMS data and the OC measured with the filter samples with 12 hours time resolution ( $PM_{2.5}$ ) is presented for the LHVP and SIRTA sites. The HR- analysis provided an average OM/OC ratio equal to  $1.58 \pm 0.11$  for LHVP and to  $1.79 \pm 0.10$  for SIRTA. In both cases the influence of the different size cut between the AMS and filters have to be taken into account. The two scatter plots present a very good linear correlation between the AMS and the filter data ( $R^2=0.85$  for the SIRTA site and  $R^2=0.92$  for the LHVP one). The AMS  $E_b$  assumed from the previous comparisons (0.5 for the SIRTA site and 0.4 for the LHVP instrument) has been applied to the AMS OC concentrations.

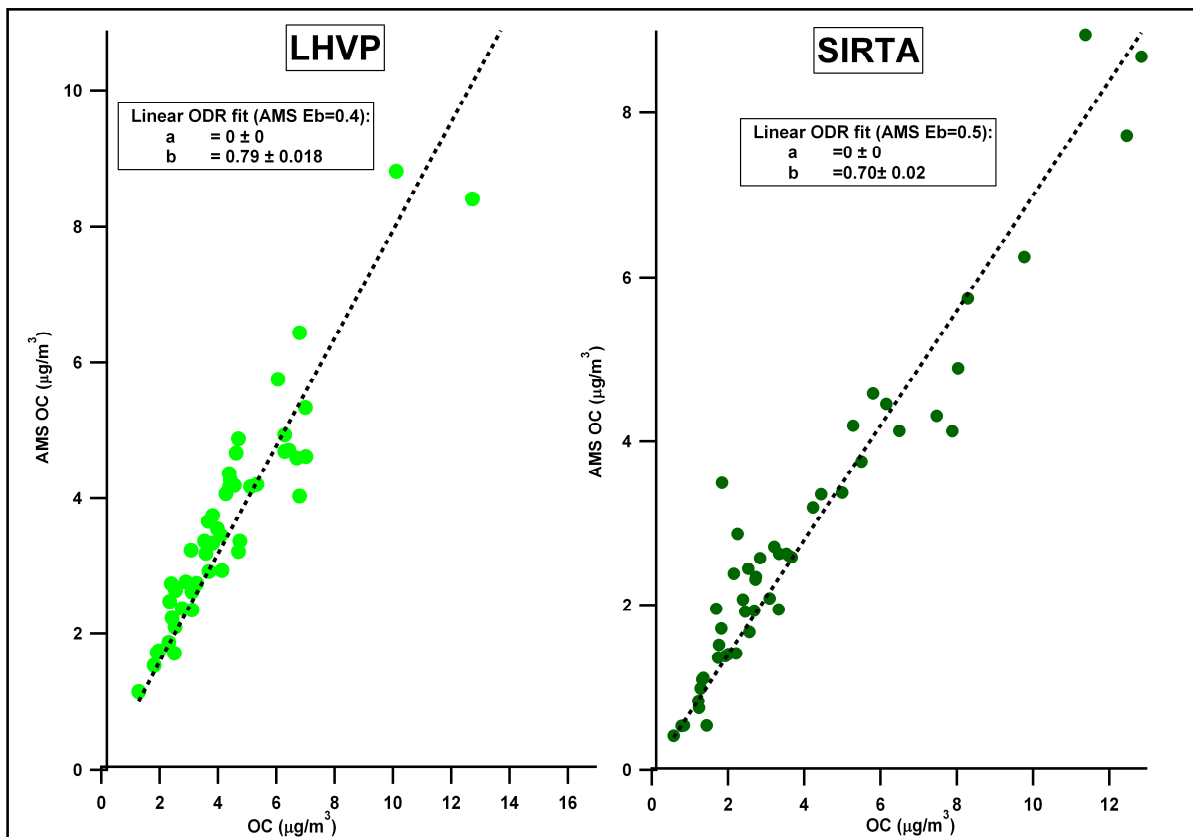


Figure SI-4:  $E_b$  estimation: OC from AMS and filter measurements.

## SI-5 PMF results in the f44 vs f43 triangle

The identified source profiles from the PMF analysis for each measurement site are represented within the triangular space defined in figure SI-5.1 (Ng et al., 2010), where  $f_{43}$  and  $f_{44}$  are the organic fractional signals at masses 43 and 44.

The purpose of Fig. SI-5.1 is to show that the identified organic sources can be grouped in different region of this triangular space, although some of the differences within each group of sources might be due to the deployment of different types of instruments (e.g. C-ToF vs HR-ToF-AMS), different ion transmission and fragmentation etc.

The BBOA components lie outside the left side of the triangle, the hydrocarbon components stay at the bottom base of the triangle due to their low oxidation state, whereas the cooking factors are in between the HOA and BBOA. Analogous results for the primary cooking sources have been obtained through smog chamber experiments (Heringa et al., 2011).

Oxidized OA moves upwards and to the left with age and oxygenation, while the OOA<sub>2</sub>-BBOA fractions are less oxidized. Uncertainties associated with the deployment of three different AMS resulting in a variability of the mass spectra of each source separated by PMF at the three sites must be taken into account in the interpretation of the  $f_{44}$  vs.  $f_{43}$  ratios (see also SI-6.6).

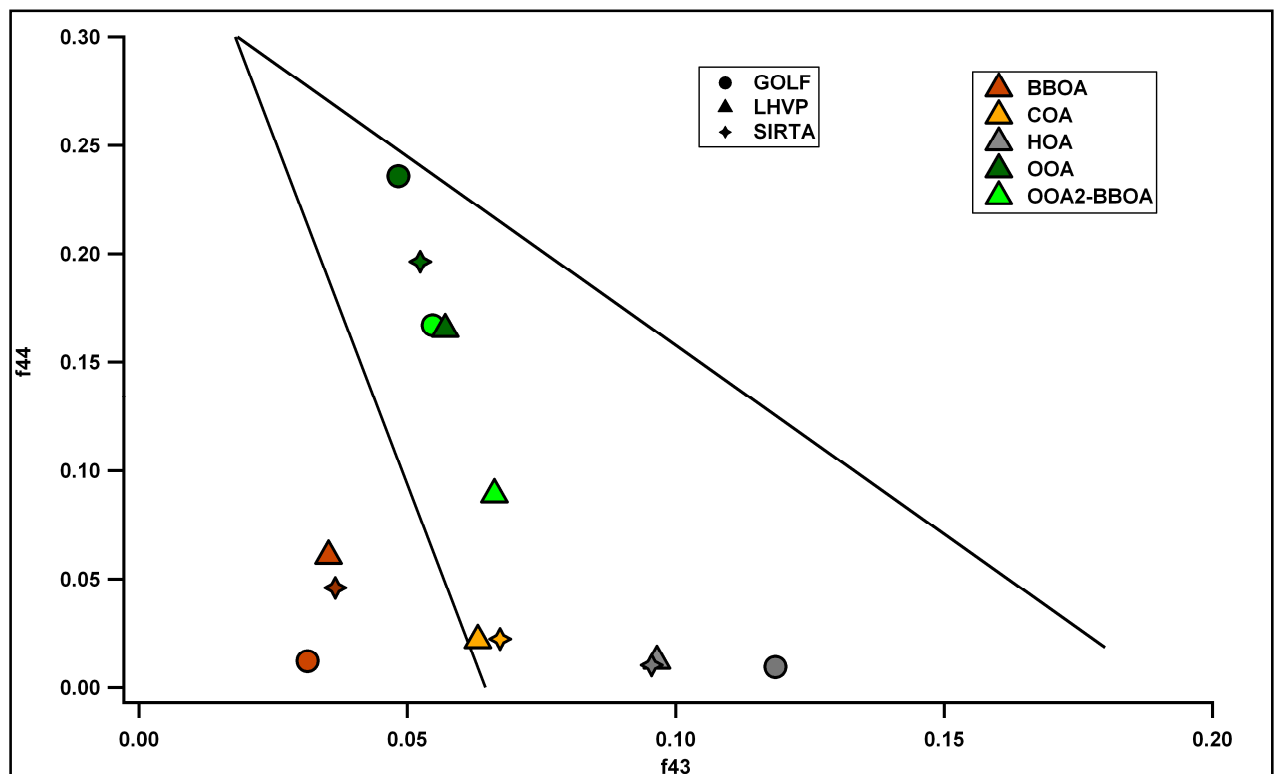


Figure SI-5.1: PMF factors in the  $f_{44}$ - $f_{43}$  triangular space.

## SI-6 PMF results

### SI-6.1 $Q/Q_{exp}$ criterion

$Q/Q_{exp}$  plots show diminishing of this ratio around 3-4 factors. The theoretical  $Q/Q_{exp}$  value is equal to 1.

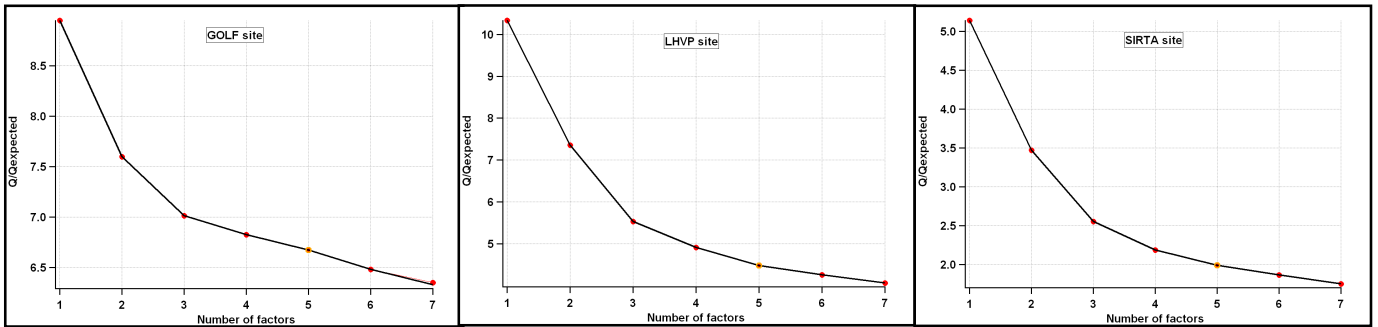


Figure SI-6.1:  $Q/Q_{exp}$  for the three sites.

### SI-6.2 PMF solutions discussion

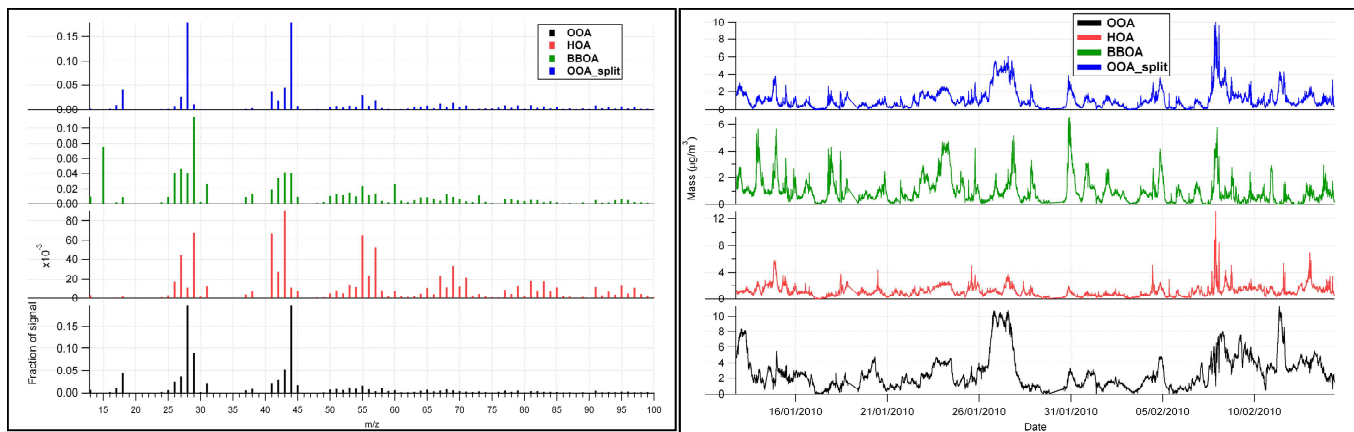


Figure SI-6.2.1: Mass spectra and time series associated with the 4 factors solution (SIRTA site).

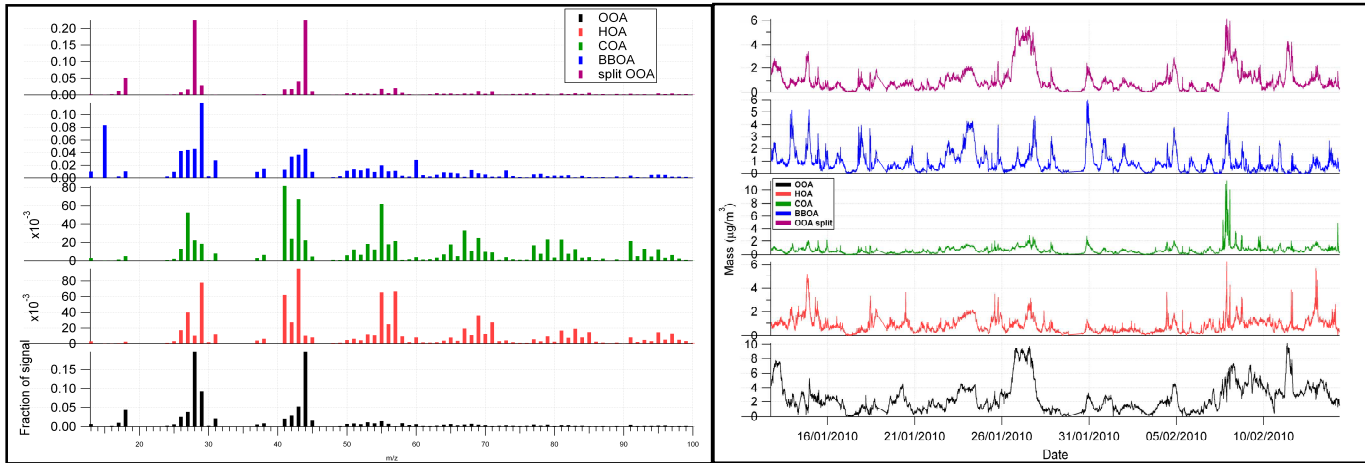


Figure SI-6.2.2: Mass spectra and time series associated with the 5 factors solution (SIRTA site).

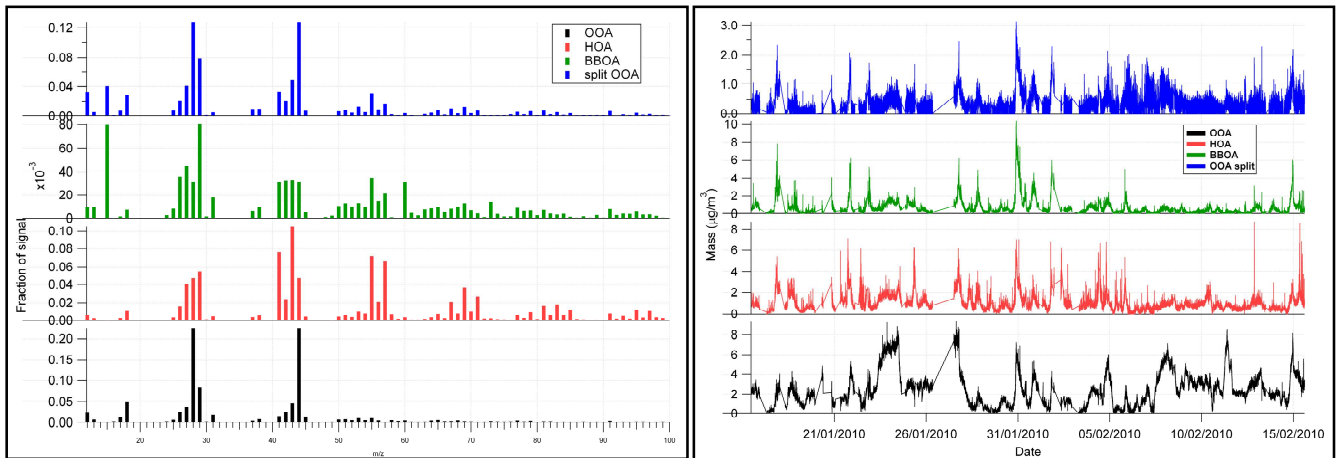


Figure SI-6.2.3: Mass spectra and time series associated with the 4 factors solution (GOLF site).

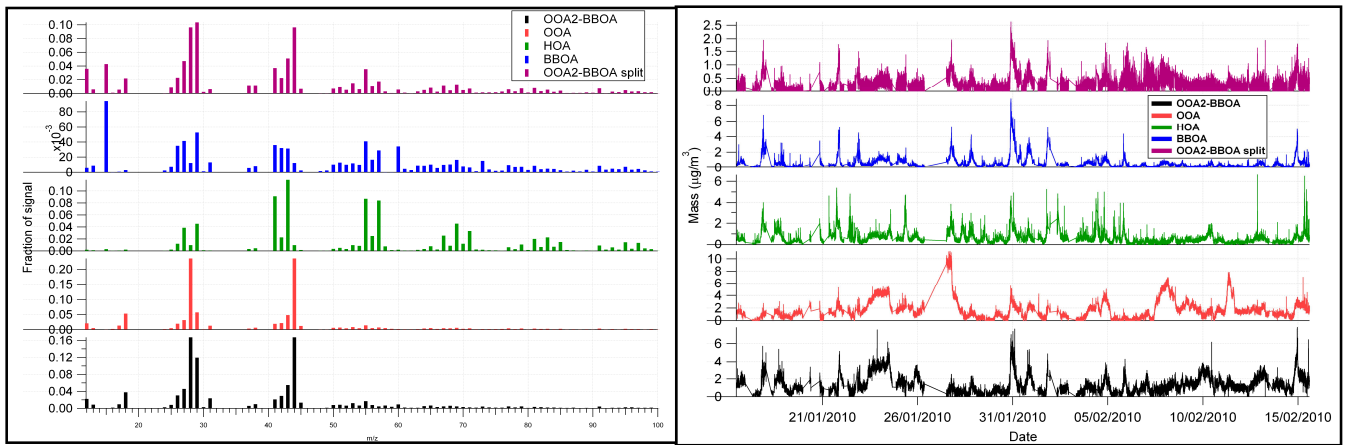


Figure SI-6.2.4: Mass spectra and time series associated with the 5 factors solution (GOLF site).

### SI-6.3 Rotational ambiguity: fpeak variation

The rotational ambiguity of the selected PMF solutions are explored for each site via the fpeak parameter in the range  $\pm 10$ .

For the LHVP site, the fpeak=0 solution provided a BBOA MS with a very small contribution at m/z44 (which should instead contribute to biomass burning sources). Additionally, a clearer distinction between the OOA and OOA<sub>2</sub>-BBOA factor was retrieved (major differences both in the time series and mass spectra). For this reason we decided to discuss within this paper the fpeak=-0.1 solution.

Figure SI-6.3.1 shows the variation of the factor relative contributions in the fpeak range -10, +10 for the LHVP site. Moving towards negative fpeaks, the split between the BBOA and OOA<sub>2</sub>-BBOA factor is disappearing and the HOA mass spectrum presents higher contributions at mass 44, especially for fpeak values below -3 (corresponding to a  $Q/Q_{exp}$  variation around 10%). Similarly, positive fpeaks (above 4) incorporated the OOA<sub>2</sub>-BBOA factor into the BBOA and OOA ones and a non-meaningful mass spectrum was obtained for highly positive fpeaks.

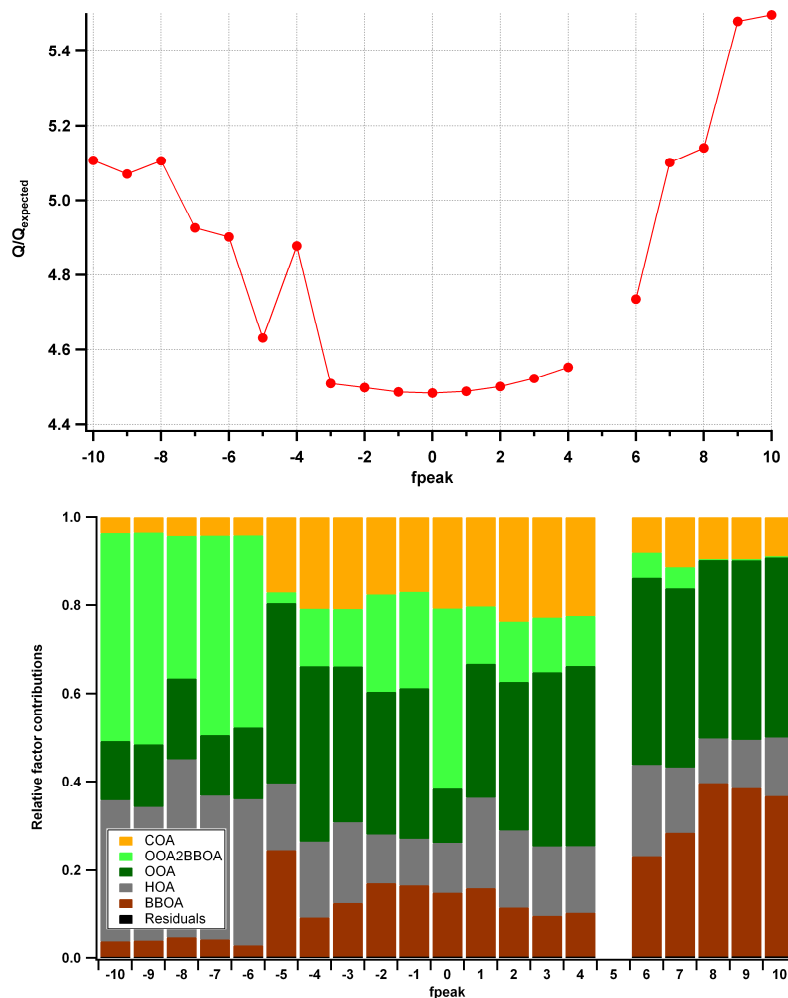


Figure SI-6.3.1: Relative factor contributions and  $Q/Q_{exp}$  as function of the  $f_{peak}$  parameter for the LHVP site.

Figure SI-6.3.2 shows the variation in the factor relative contributions in the  $f_{peak}$  range -10, +10 for the SIRTA site. Strongly negative  $f_{peak}$ s affect the separation of a cooking factor, in fact below  $f_{peak}=-4$  the COA contribution disappears. Very positive  $f_{peak}$ s affect the separation of OOA and BBOA, providing a split of the BBOA factor and not a separation of two OOA components.

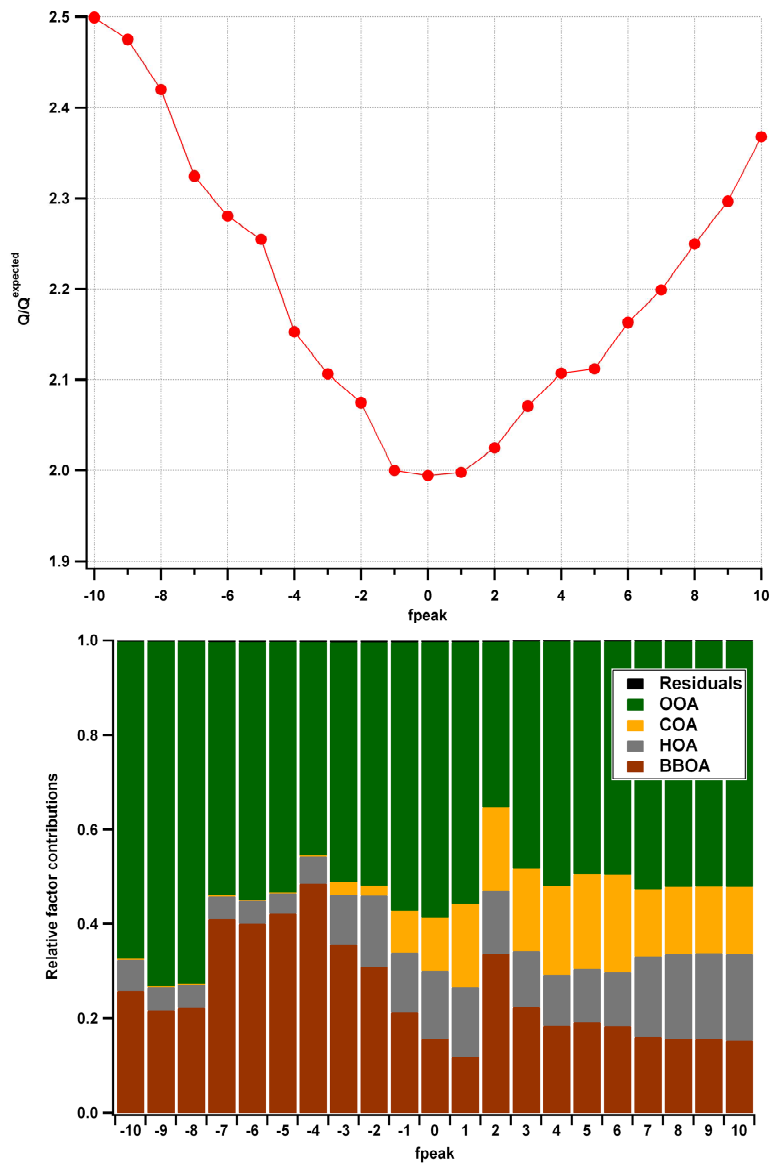


Figure SI-6.3.2: Relative factor contributions and  $Q/Q_{exp}$  as function of the  $f_{peak}$  parameter for the SIRTA site.

Figure SI-6.3.3 shows the variation in the factor relative contribution in the fpeak range -10, +10 for the GOLF site. The separation of the OOA<sub>2</sub>-BBOA and OOA factors is fpeak dependent and affected by both negative and positive fpeaks. Negative fpeaks produced often non reasonable time series, while positive fpeaks influenced mainly the mass spectra.

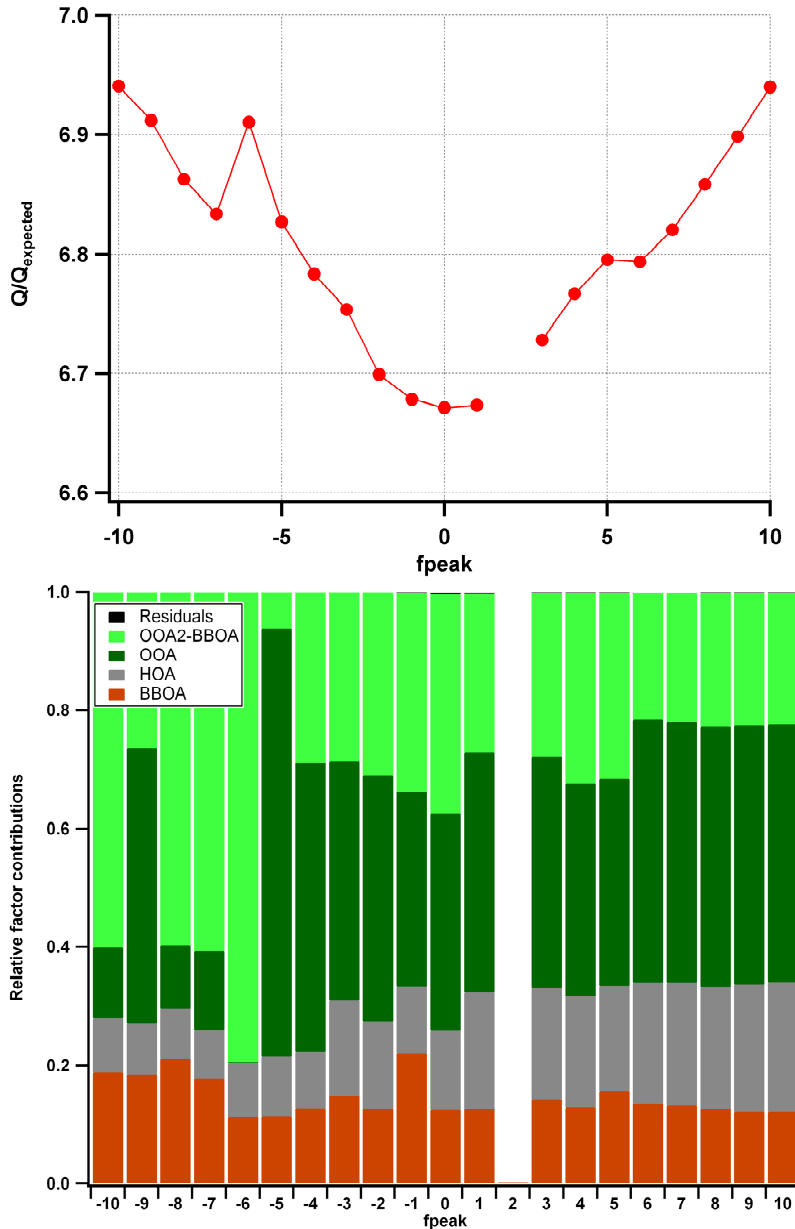


Figure SI-6.3.3: Relative factor contributions and  $Q/Q_{\text{exp}}$  as function of the fpeak parameter for the GOLF site.

### SI-6.4 Local minima investigation: seeds variation

To investigate the possibility of local minima in the PMF solution space, the algorithm was initialized using 50 different starting points (“seeds”). Figures SI-6.4.1, SI-6.4.2 and SI-6.4.3 show the variation of the relative sources contributions and of the  $Q/Q_{exp}$  parameter as a function of seed for the SIRTA, LHVP and GOLF sites respectively.

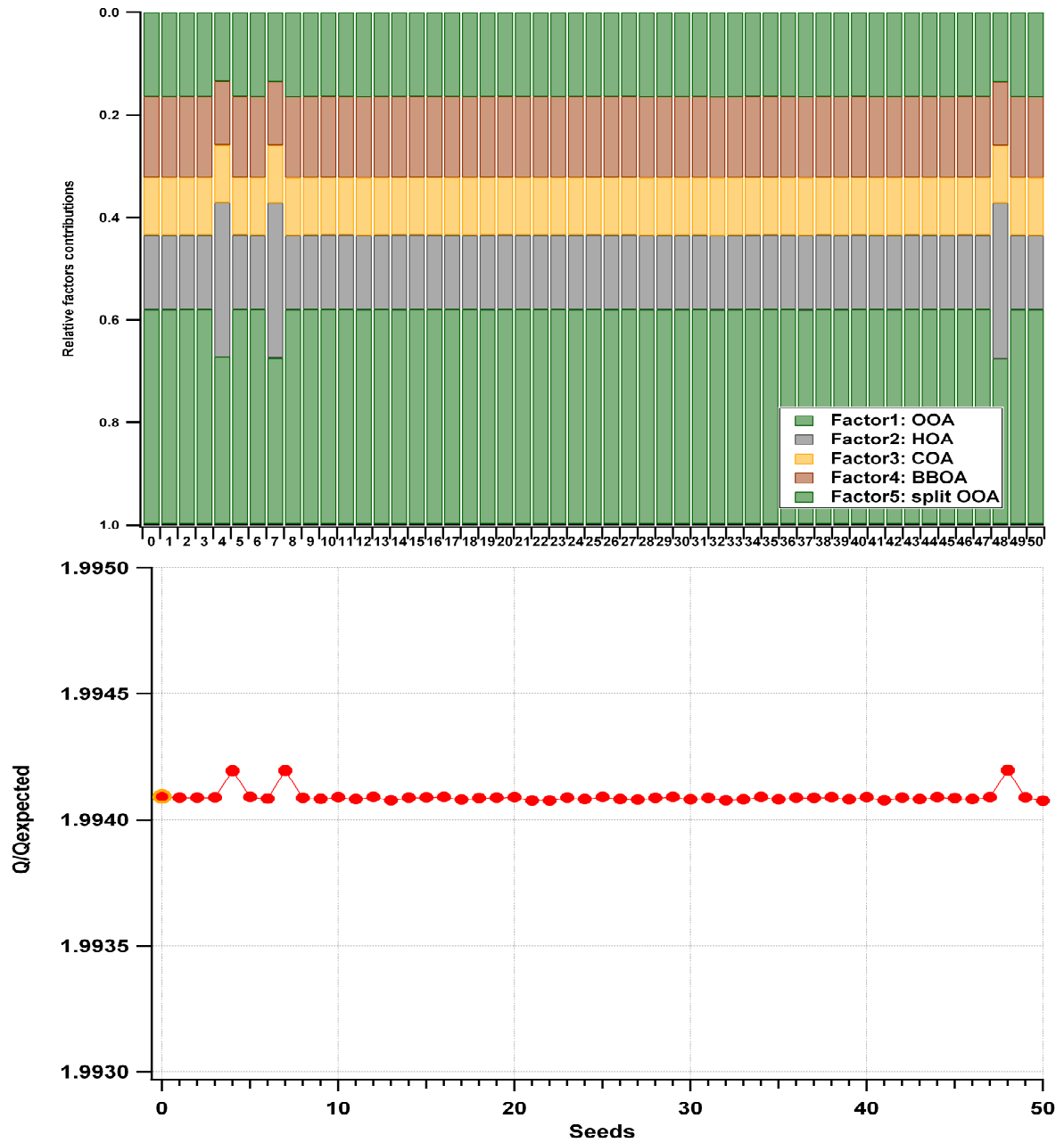


Figure SI-6.4.1: Relative factors contribution as function of different seeds (SIRTA site). The solution is stable using 50 different starting points. The GOLF station seed analysis provided 2 groups of solutions characterized by different values of the ratio  $Q/Q_{exp}$ , as shown in Fig. SI-6.4.2. The two groups of solutions are mostly similar (Fig. SI-6.4.3). However, those with “higher”  $Q/Q_{exp}$  values are characterized by higher org44 in the HOA spectrum compared to the other group. In addition the switch between the 2 groups of solutions is associated also with different interpretation of the PMF factors. Considering the “lower”  $Q/Q_{exp}$  solutions the interpretation of the source spectra is OOA, HOA, BBOA, OOA<sub>2</sub>-BBOA and split of OOA<sub>2</sub>-BBOA moving from factor1 to factor5, whereas it is OOA, OOA<sub>2</sub>-BBOA, HOA, BBOA and split of OOA<sub>2</sub>-BBOA for the “higher”  $Q/Q_{exp}$  ratios.

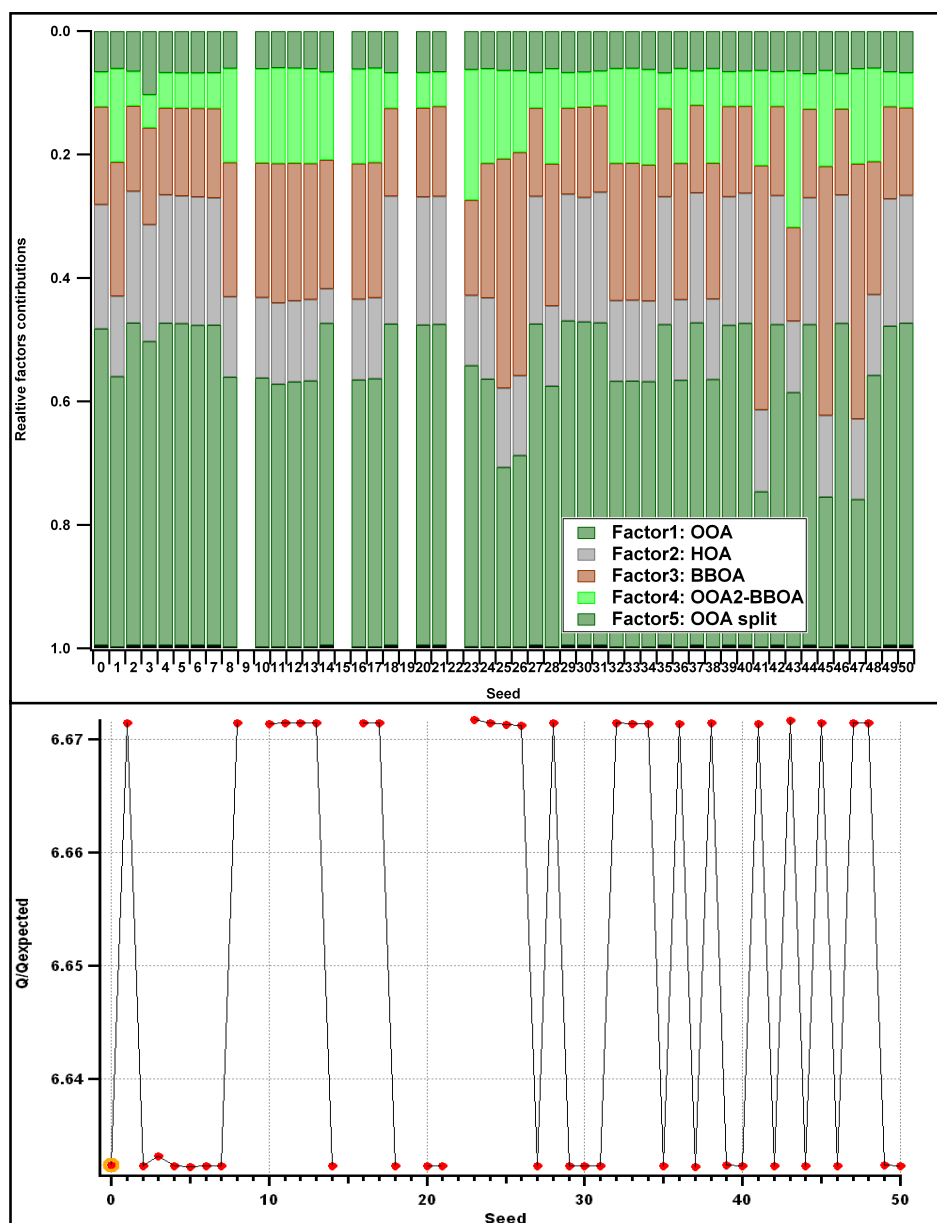


Figure SI-6.4.2: Relative factors contribution as function of different seeds (GOLF).

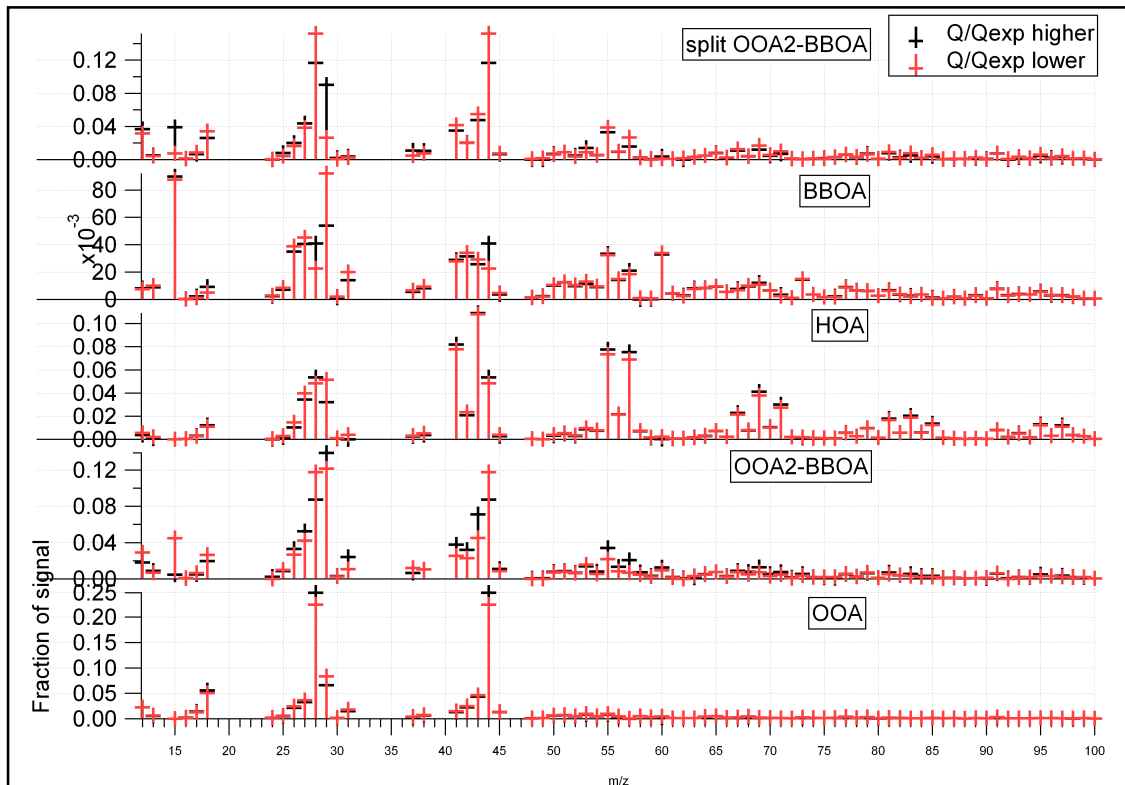


Figure SI-6.4.3: Mass spectra comparison of different  $Q/Q_{exp}$  solutions (GOLF).

The analysis of the seeds variation for the LHVP dataset gave 2 groups of solutions characterized by different values of the ratio  $Q/Q_{exp}$  shown in Fig. SI-6.4.4.

The solutions with “higher”  $Q/Q_{exp}$  values are not completely physically meaningful since the BBOA spectrum does not show org44 in the mass spectrum and the OOA<sub>2</sub>-BBOA profile is less clear than the one from the other group (Fig. SI-6.4.5). In addition a different interpretation of the PMF factors can be seen between the 2 groups of solutions.

Considering the “high”  $Q/Q_{exp}$  solutions the interpretation of the source spectra is OOA<sub>2</sub>-BBOA, COA, HOA, BBOA and OOA moving from factor1 to factor5, whereas it is COA, OOA<sub>2</sub>-BBOA, OOA, HOA and BBOA for the lower  $Q/Q_{exp}$  ratios.

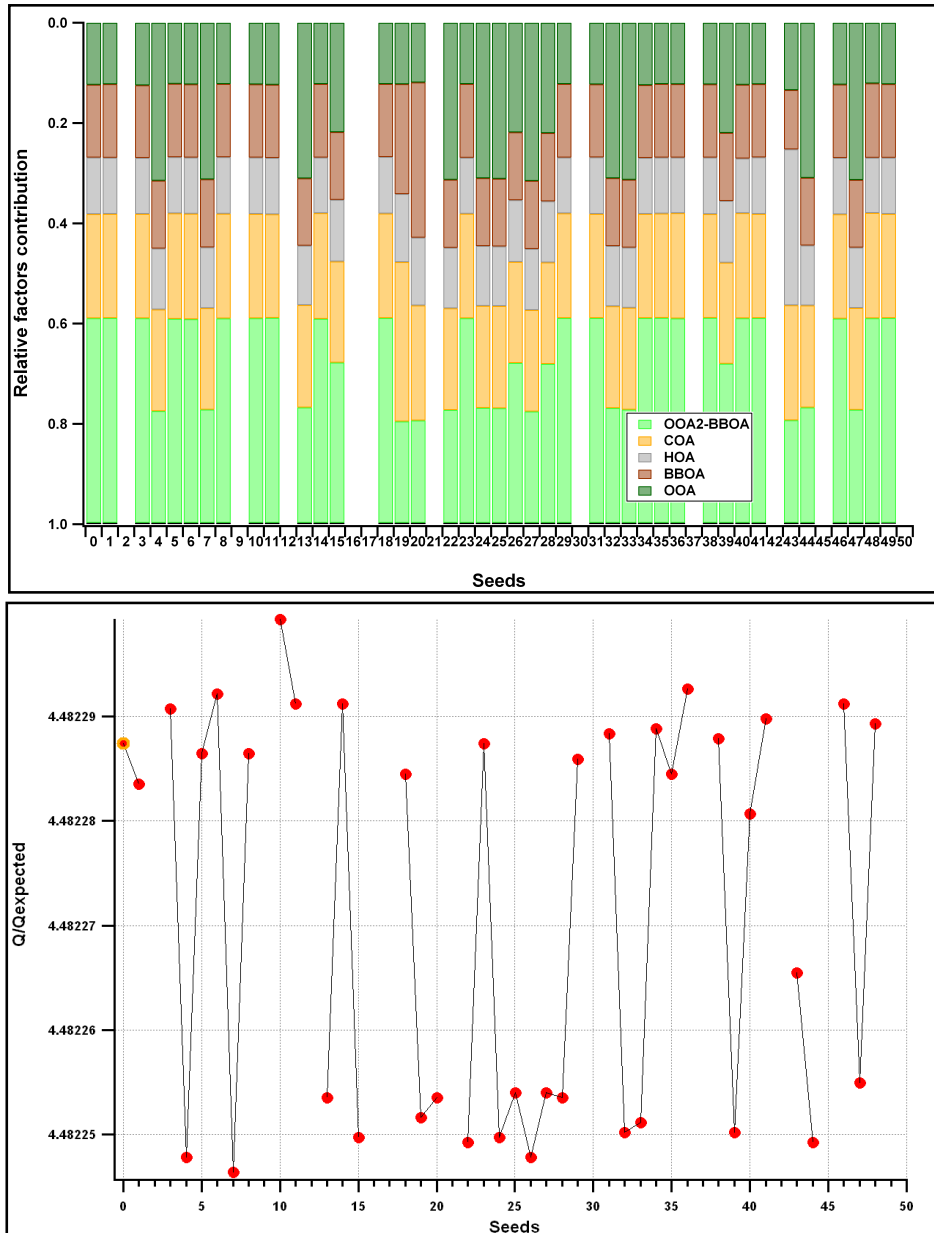


Figure SI-6.4.4: Relative factor contributions as function of different seeds (LHVP).

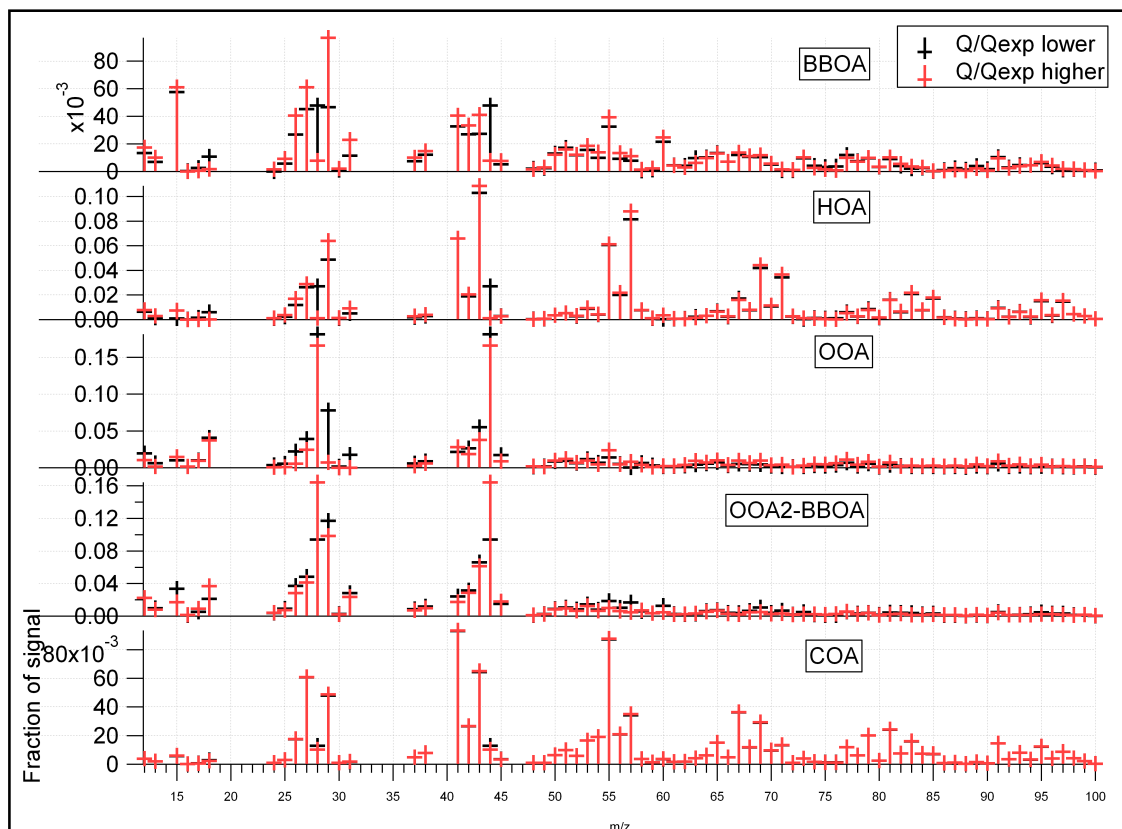


Figure SI-6.4.5: Mass spectra comparison of different Q/Qexp solutions (LHVP).

### SI-6.5 PMF solution residuals

Figures SI-6.5.1, SI-6.5.2, SI-6.5.3 represent the residuals of the PMF algorithm in terms of time series and mass spectra. Significantly important to evaluate the performance of the model are the scaled residuals graphs (both in terms of time series and mass spectra) which represent what the model was not able to describe. At all the three stations PMF residuals are on average quite low.

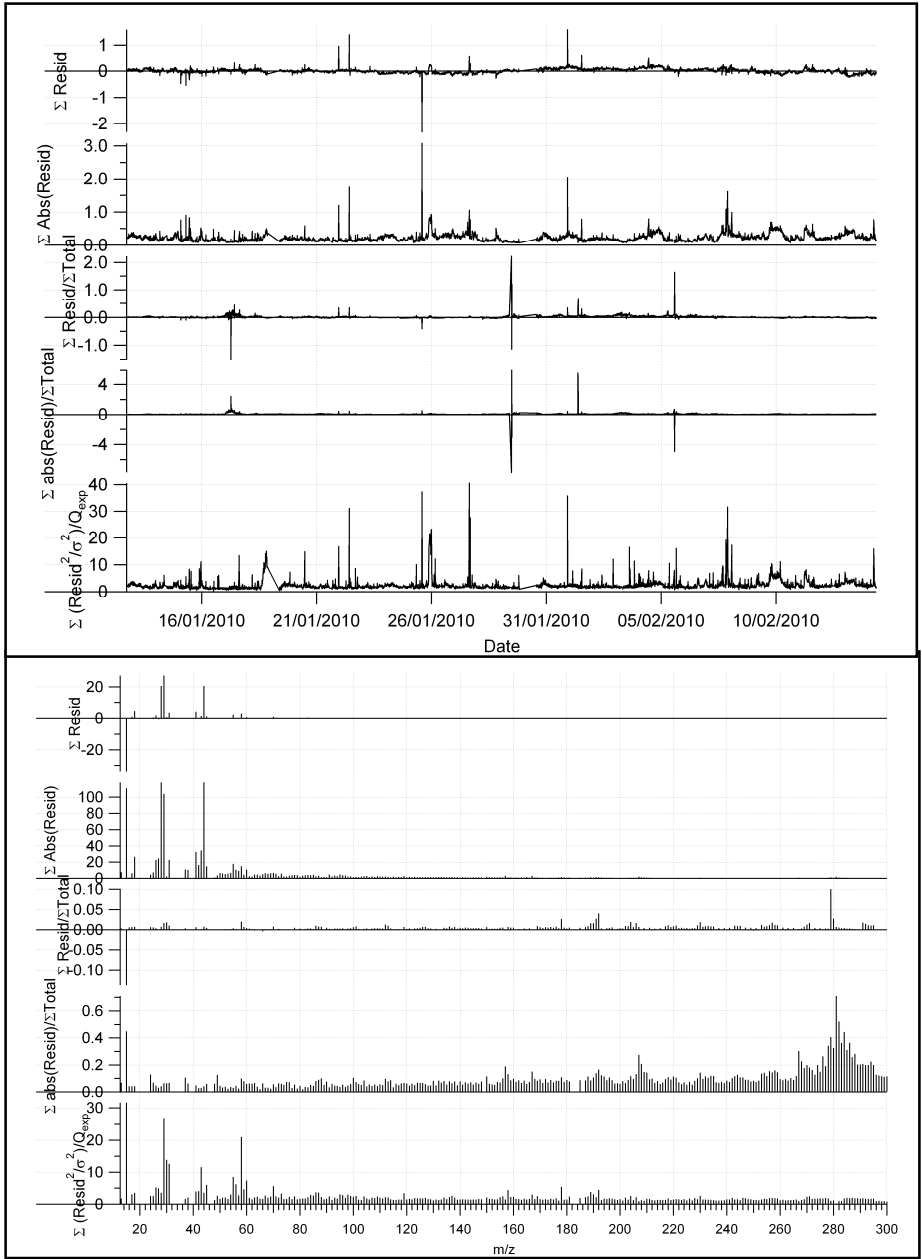


Figure SI-6.5.1: Residual time series and mass spectra (SIRTA).

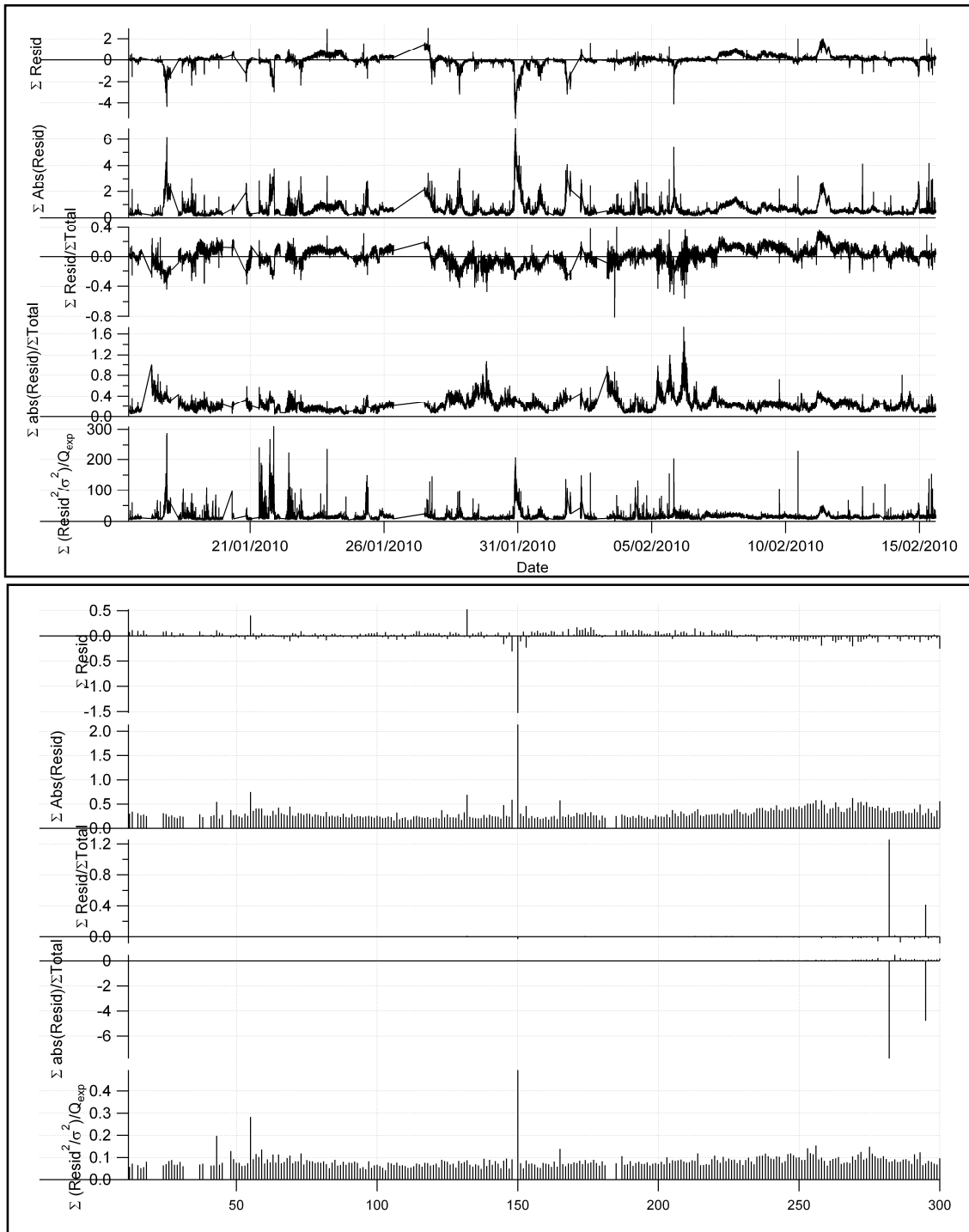


Figure SI-6.5.2: Residual time series and mass spectra (GOLF).

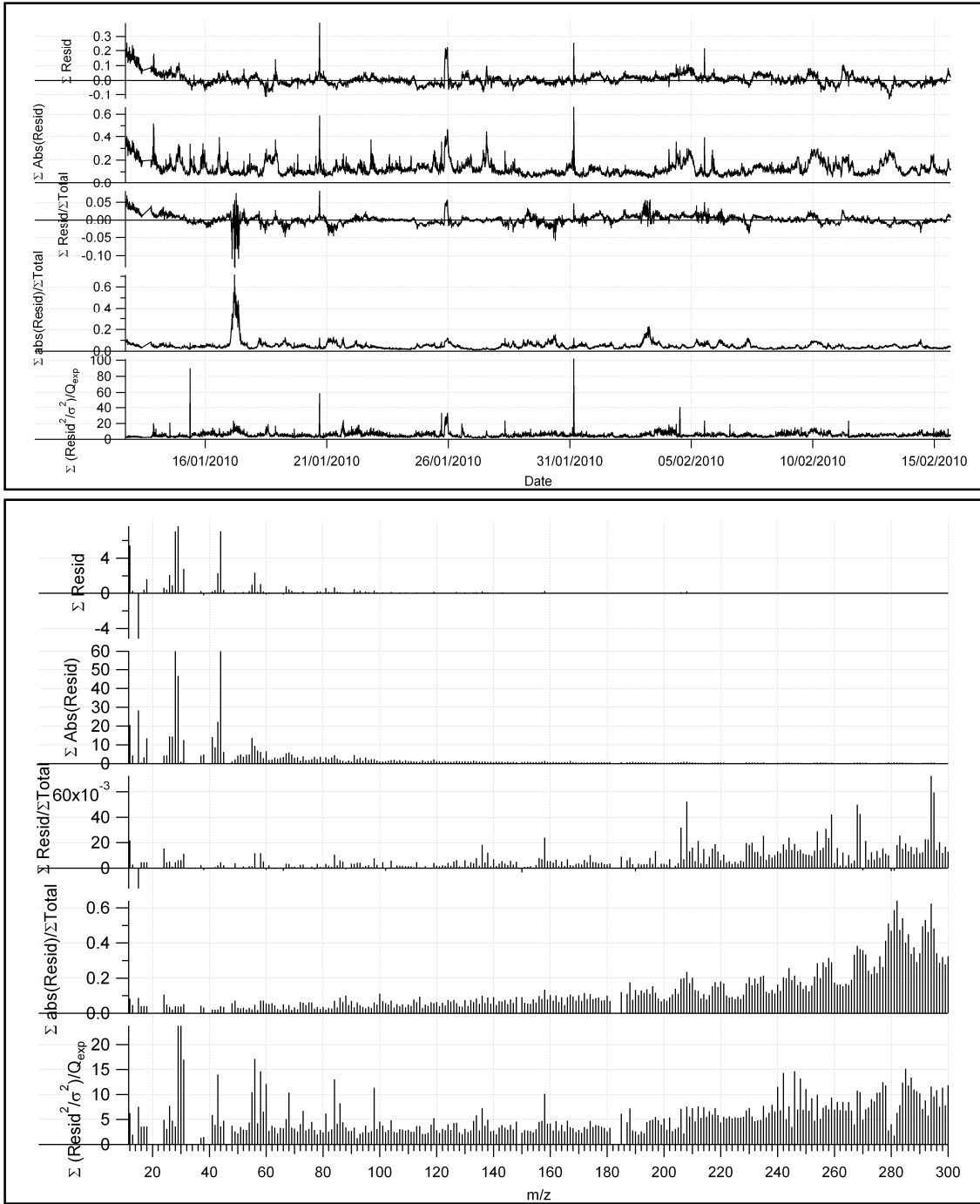


Figure SI-6.5.3: Residual time series and mass spectra (LHVP).

## SI-6.6 Tracers of cooking and biomass burning sources

The relative contribution of the biomass burning factor separated by PMF at the three sites is compared with the fraction of organic60 to the total organic mass ( $f_{60}$ ), as sensitive quantity for BBOA.

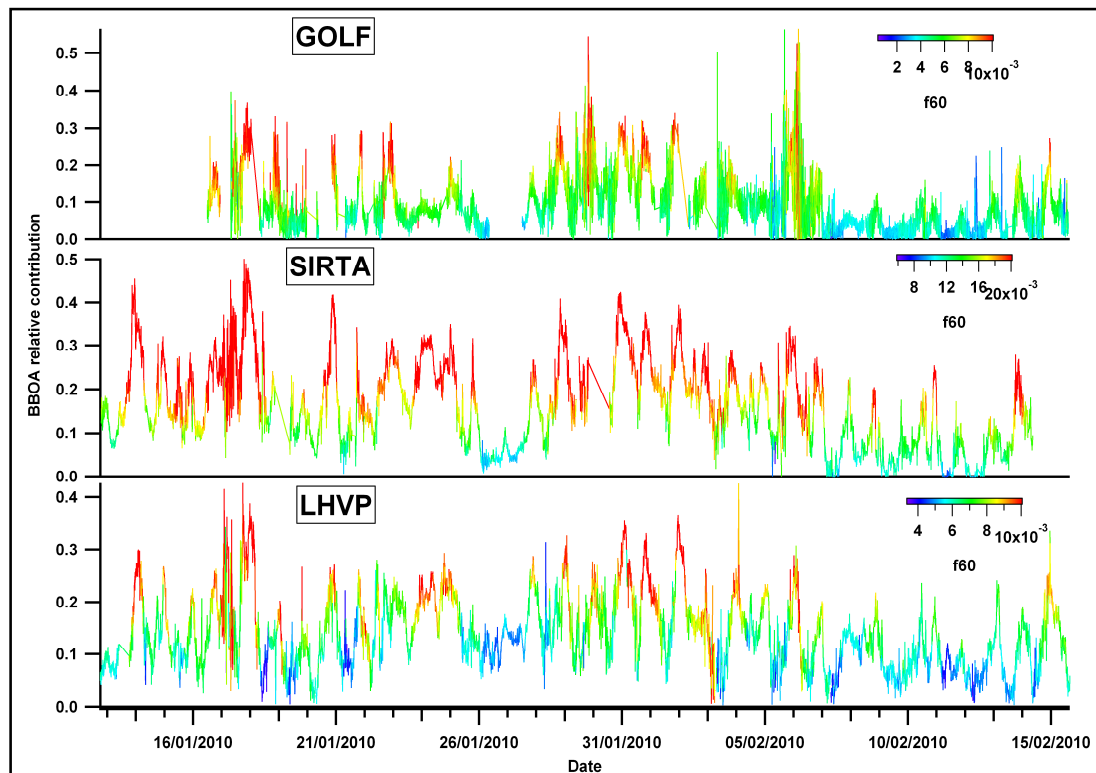


Figure SI-6.6.1: Relative contribution of organic60 as tracer of biomass burning aerosols.

The relative contribution of the cooking factor separated by PMF at the SARTA and LHVP sites is compared with the organic ratio at mass 55 to organic at mass 57 ( $org_{55}/org_{57}$ ). The ratio  $org_{55}/org_{57}$  represents a robust marker for COA as introduced by Mohr et al. (2012). The contributions at organic masses 55 and 57 apportioned to the OOA factors have been subtracted when calculating the ratio  $org_{55}/org_{57}$ .

The relative fraction of cooking is never reaching as high values at SARTA compared to LHVP. In rural areas, the  $org_{55}/org_{57}$  approach will be much more uncertain as also OOA contributes to a higher degree to these mass fragments compared to urban areas.

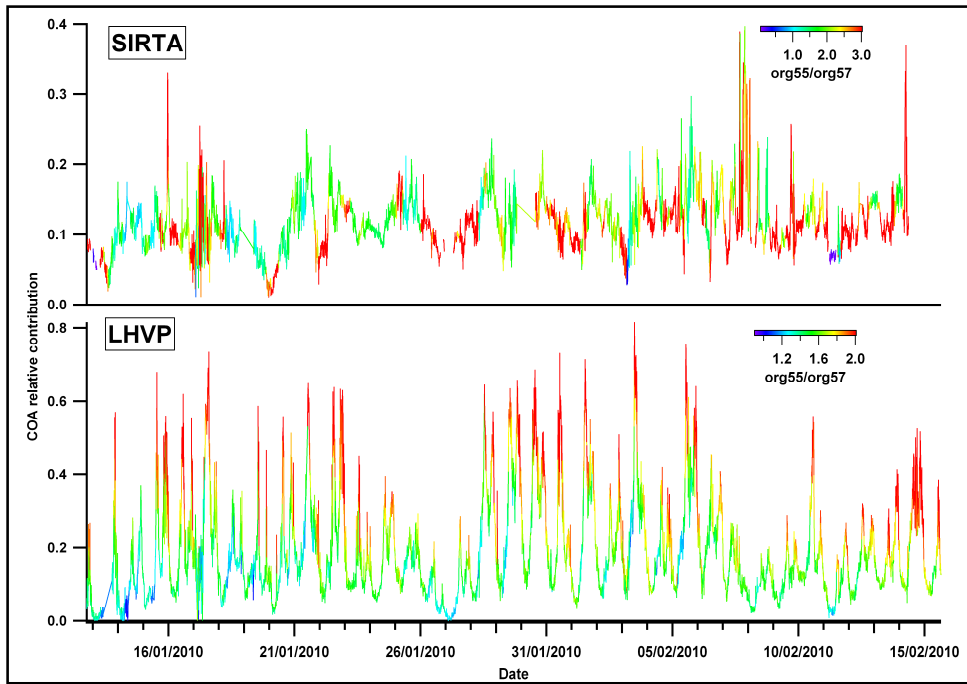


Figure SI-6.6.2: Ratio of organic55 to organic57 as tracer of cooking aerosols.

### SI- 6.7 Intercomparison of PMF solutions at the 3 sites

A comparison of the PMF results obtained at the three sites in terms of mass spectra and time series is represented in Figure SI-6.7.1. The mass spectra of the identified sources are quite stable among the sites; however the differences at masses 15, 29 and 44 are most probably associated to the use of several AMS, as discussed in section SI-3. Oxidized organic aerosols indicate a homogeneous temporal variation over the Parisian region, while the role of local primary emission sources can be identified in the time variability of HOA and COA. The wood burning emissions appear to have a regional behavior, although several local spikes can be identified.

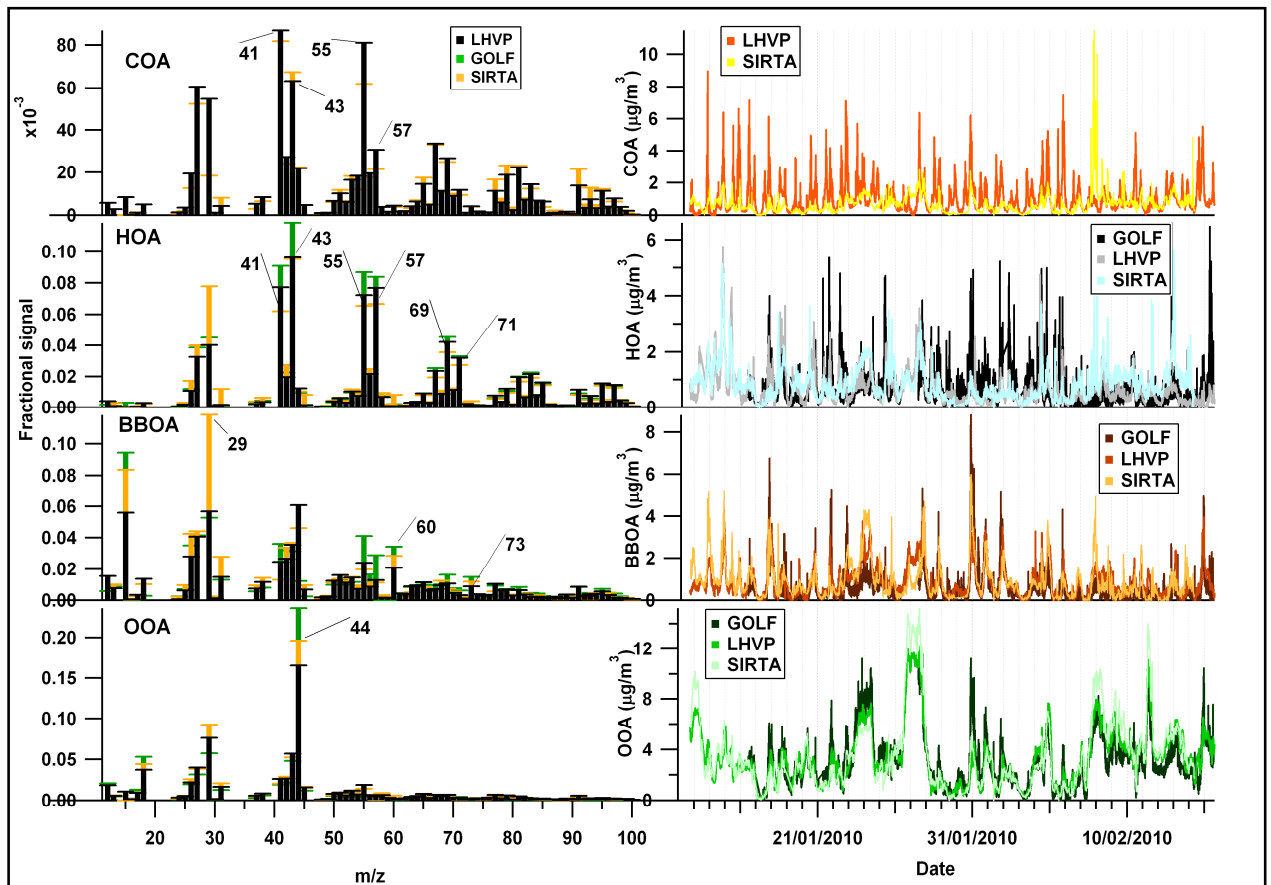


Figure SI-6.7.1: PMF results over the Paris region.

**SI-7 Comparison of black carbon measurements at SIRTA and in a remote rural site**

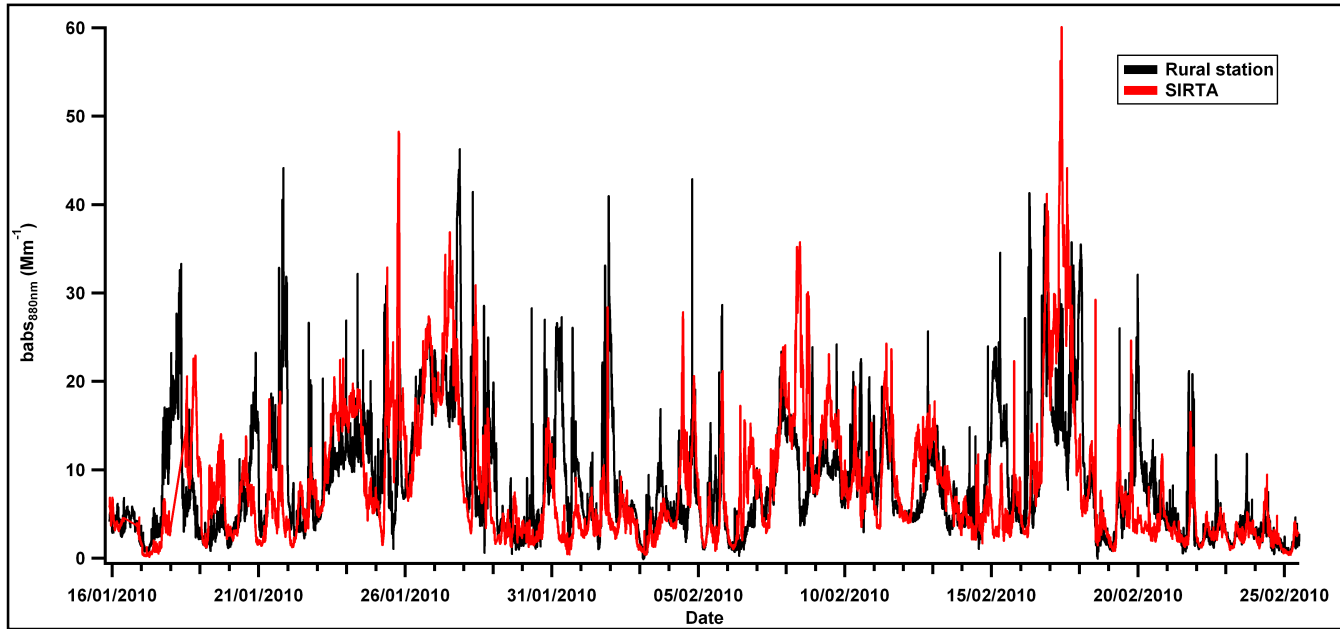


Figure SI-7: Comparison of the black carbon absorption coefficients measured at the SIRTA site and in a remote rural location by two aethalometers.

## SI-8 Back trajectories for specific events

Back trajectories ending at the SIRTAsite have been evaluated using HYSPLIT (Hybrid Single Particle Lagrangian Integrated Trajectory Model) at an initial altitude of 500 meters with a total run time for each day trajectory of 48 hours (Draxler, 1997, 1998). The vertical motion was considered isobaric and the meteorological information has been obtained from the GDAS database.



Figure SI-8: Back trajectories of specific events.

## References

- Bahreini, R., Ervens, B., Middlebrook, A. M., Warneke, C., de Gouw, J. A., DeCarlo, P. F., Jimenez, J. L., Brock, C. A., Neuman, J. A., Ryerson, T. B., Stark, H., Atlas, E., Brioude, J., Fried, A., Holloway, J. S., Peischl, J., Richter, D., Walega, J., Weibring, P., Wollny, A. G., and Fehsenfeld, F. C.: Organic aerosol formation in urban and industrial plumes near Houston and Dallas, Texas, *Journal of Geophysical Research*, 114, D00F16, doi: 10.1029/2008JD011493, 2009.
- Draxler, R. R., and G.D. Hess: Description of the HYSPLI4 modeling system, NOAA Tech. Memo. , Environ. Res. Lab., Boulder, Colo., ERL ARL-224, 24, 1997.
- Draxler, R. R., and G.D. Hess: An Overview of the HYSPLI4 modeling system for trajectories, dispersion and deposition, *Aust. Meteorol. Mag.*, 47, 295-308, 1998.
- Drewnick, F., Böttger, T., Von der Weiden-Reinmüller, S.-L., Zorn, S.R., Klimach, T., Schneider, J., Borrmann, S. : Design of a mobile aerosol research laboratory and data processing tools for effective and high-resolution field measurements, *Atmos. Meas. Tech.*, 5, 1443-1457, 2012.
- Duplissy, J., DeCarlo, P. F., Dommen, J., Alfarra, M. R., Metzger, A., Barmpadimos, I., Prevot, A. S. H., Weingartner, E., Tritscher, T., Gysel, M., Aiken, A. C., Jimenez, J. L., Canagaratna, M. R., Worsnop, D. R., Collins, D. R., Tomlinson, J., and Baltensperger, U.: Relating hygroscopicity and composition of organic aerosol particulate matter, *Atmos. Chem. Phys.*, 11, 1155-1165, 2011.
- Freutel, F., Schneider, J., Drewnick, F., von der Weiden-Reinmüller, S.-L., Crippa, M., Prévôt, A. S. H., Baltensperger, U., Poulain, L., Wiedensohler, A., Sciare, J., Sarda-Estève, R., Burkhardt, J. F., Eckhardt, S., Stohl, A., Gros, V., Colomb, A., Michoud, V., Doussin, J. F., Borbon, A., Haefelin, M., Morille, Y., Beekmann, M., and S., a. B.: Aerosol particle measurements at three stationary sites in the megacity of Paris during summer 2009: Meteorology and air mass origin dominate aerosol particle composition and size distribution, *ACP*, 13, 1–27, 2013.
- Heringa, M. F., DeCarlo, P. F., Chirico, R., Tritscher, T., Dommen, J., Weingartner, E., Richter, R., Wehrle, G., Prévôt, A. S. H., and Baltensperger, U.: Investigations of primary and secondary particulate matter of different wood combustion appliances with a high-resolution time-of-flight aerosol mass spectrometer, *Atmos. Chem. Phys.*, 11, 5945-5957, 2011.
- Matthew, B. M., Middlebrook, A. M., and Onasch, T. B.: Collection efficiencies in an Aerodyne aerosol mass spectrometer as a function of particle phase for laboratory generated aerosols, *Aerosol Sci. Technol.*, 42, 884-898, 2008.

Middlebrook, A. M., Bahreini, R., Jimenez, J. L. and Canagaratna, M. R.: Evaluation of composition-dependent collection efficiencies for the Aerodyne aerosol mass spectrometer using field data, *Aerosol Sci. Technol.*, 46:3, 258-271, 2012.

Mohr, C., Richter, R., DeCarlo, P. F., Prevot, A. S. H., and Baltensperger, U.: Spatial variation of chemical composition and sources of submicron aerosol in Zurich during wintertime using mobile aerosol mass spectrometer data, *Atmos. Chem. Phys.*, 11, 7465-7482, 2011.

Mohr, C., DeCarlo, P. F., Heringa, M. F., Chirico, R., Slowik, J. G., Richter, R., Reche, C., Alastuey, A., Querol, X., Seco, R., Peñuelas, J., Jiménez, J. L., Crippa, M., Zimmermann, R., Baltensperger, U., and Prévôt, A. S. H.: Identification and quantification of organic aerosol from cooking and other sources in Barcelona using aerosol mass spectrometer data, *Atmos. Chem. Phys.*, 12, 1649-1665, 2012.

Ng, N. L., Canagaratna, M. R., Zhang, Q., Jimenez, J. L., Tian, J., Ulbrich, I. M., Kroll, J. H., Docherty, K. S., Chhabra, P. S., Bahreini, R., Murphy, S. M., Seinfeld, J. H., Hildebrandt, L., Donahue, N. M., DeCarlo, P. F., Lanz, V. A., Prevot, A. S. H., Dinar, E., Rudich, Y., and Worsnop, D. R.: Organic aerosol components observed in Northern Hemispheric datasets from aerosol mass spectrometry, *Atmos. Chem. Phys.*, 10, 4625-4641, 2010.

Von der Weiden-Reinmüller, S.-L., Drewnick, F., Crippa, M., Prévôt, A.S.H., Meleux, F., Böttger, T., Zorn, S.R., Diesch, J.-M., Baltensberger, U., Beekmann, M., Borrmann, S.: On the applicability of mobile aerosol and trace gas measurements for the investigation of characteristics and transformation of megacity emissions: The Paris metropolitan area, in preparation.